UCRL-17453

cy.2

University of California

Ernest O. Lawrence Radiation Laboratory

AN EPR STUDY OF THE $O_2(^1\Delta_g)$ MOLECULE

Arnold M. Falick

June 1967

DISCLAIMER

UCRL-17453

UNIVERSITY OF CALIFORNIA

Lawrence Radiation Laboratory
Berkeley, California

AEC Contract No. W-7405-eng-48

AN EPR STUDY OF THE $O_2(^1\Delta_g)$ MOLECULE

Arnold M. Falick

(Ph.D. Thesis)

June 1967

TABLE OF CONTENTS

AN EPR STUDY OF THE $O_2(^1\Delta_g)$ MOLECULE

Arnold M. Falick

Inorganic Materials Research Division, Lawrence Radiation Laboratory,
Department of Chemistry, University of California
Berkeley, California

ABSTRACT

June 1967

The 4-line EPR spectrum of the J=2 level of the $O_2(^1\Delta_g)$ molecule in discharged oxygen produced in a 13.56 MHz discharge-flow system has been measured and analyzed. The calculated spectrum gives an excellent fit to the experimental one by using $g_J = -0.66662$. Transition matrix elements have been calculated for the $O_2(^1\Delta_g)$ EPR transitions so that absolute concentration measurements could be made.

The rate of the reaction

$$O_2(^1\Delta_g) + O_2(^1\Delta_g) \rightarrow 2O_2(^3\Sigma_g^-) + h\nu \ (6340\ A) \qquad (1)$$

was measured as a function of pressure over the range 0.1-1.0 torr and in mixtures of oxygen with up to 75% of He and Ar. The 6340 A emission, which was detected with an interference filter and an RCA 7265 photomultiplier, was found to be second order with respect to $O_2(^1\Delta_g)$ concentration under all of the experimental conditions used. The $O_2(^1\Delta_g)$ concentration was determined from the intensity of one of its EPR lines, and absolute concentrations were calculated by comparison with $O_2(^3\Sigma_g^-)$ ground state EPR lines. The second order rate constant for reaction (1) did not change with pressure or added gas and was found to be $k_1 = 5.0 \pm 0.5 \times 10^{-23}$ cm^3/molecule-sec, compared to the value of

$k_1 = 2.3 \times 10^{-22}$ cm^3/molecule-sec obtained by Ogryzlo, et al.[1] The results suggest that the reaction occurs via an O_4^* intermediate which is simply a colliding pair of excited oxygen molecules.

In addition it was found that $O_2(^1\Delta_g)$ is primarily formed in the discharge and that it reacts slowly or not at all with NO or NO_2.

---

1. J. S. Arnold, R. J. Browne and E. A. Ogryzlo, Photochem. and Photobiol. 4, 963 (1965).

I. INTRODUCTION

It has been known for a number of years that when a stream of oxygen is passed through a discharge a sizable concentration of oxygen atoms can be produced.[1] More recently, it has been established that considerable numbers of electronically excited molecules are also present in the gas stream.[2-6] Most of these excited molecules have been shown to be $O_2(^1\Delta_g)$,[2,3,7] a surprisingly durable metastable state which may comprise as much as 10% of the total pressure. A few tenths of a percent of $O_2(^1\Sigma_g^+)$, also metastable but not as long lived, will also usually be present.[7-9]

The $^1\Delta_g$ state of O_2 is the lowest excited electronic state, lying 0.98 eV above the ground $^3\Sigma_g^-$ state.[10] Its remarkable stability can be attributed to the fact that the electric dipole transition to the ground state is doubly forbidden ($g \rightarrow g$ and singlet $\rightarrow$ triplet intercombinations are forbidden for electric dipole transitions).[10] The observed emission results from a magnetic dipole transition.[11] It is weaker than the $O_2(^1\Sigma_g^+ \rightarrow {}^3\Sigma_g^-)$ emission, which is also magnetic dipole, because of the (non-rigorous) selection rule $\Delta\Lambda = 0, \pm 1$ which should hold for both electric and magnetic dipole transitions.[12]

Several interesting properties of $O_2(^1\Delta_g)$ have been reported by a number of workers. It reacts slowly or not at all with a large number of compounds including water, carbon dioxide, ammonia, hydrogen bromide, nitrogen dioxide, dimethyl ether and a good many others.[7,13] It reacts readily with unsaturated hydrocarbons and its use has been suggested as a preparative method for organic peroxides.[14-16] Left to itself, the molecule undergoes radiative decay to the ground state with a

half-life of approximately 45 min.[17] Other reactions of $O_2(^1\Delta_g)$ are particularly important in upper atmosphere chemistry and physics; it reacts rapidly with ozone to produce oxygen atoms[18] and it can undergo a type of disproportionation reaction to produce $O_2(^1\Sigma_g^+)$ and ground state oxygen.[13,19]

The experiments described in this work are related to recent spectroscopic studies of the afterglow in oxygen discharge-flow systems which produced evidence of some interesting red emission bands whose origin could not be traced to any of the known transitions of $O_2(^1\Delta_g)$ or $O_2(^1\Sigma_g^+)$. Broida et al.[20] reported a broad band at about 6200 A which was not identified. Bader and Ogryzlo[7] observed two broad structureless bands at 6340 and 7030 A from discharged oxygen which were identical with bands observed earlier in the reaction of aqueous hydrogen peroxide with chlorine,[21,22] and also with bands observed subsequently in other oxygen producing reactions.[23] They found that the intensity of the 6340 A band was proportional to the square of the $O_2(^1\Delta_g)$ concentration. Noting also the fact that a 6340 A photon has almost exactly twice the excitation energy of $O_2(^1\Delta_g)$, Bader and Ogryzlo[7] proposed the following energy pooling processes to account for the two bands:

$$2O_2(^1\Delta_g) \rightleftharpoons O_4^* \rightarrow 2O_2(^3\Sigma_g^-)_{v=0} + h\nu \text{ (6340 A)} \quad (1)$$

$$\rightarrow O_2(^3\Sigma_g^-)_{v=0} + O_2(^3\Sigma_g^-)_{v=1} + h\nu \text{ (7030 A)}. \quad (2)$$

where v is the vibrational quantum number. The temperature dependence of the emission was measured and the results led to the conclusion that

the intermediate O_4^* was a stabilized dimolecular complex with a dissociation energy of 600 cal.[7] However, this temperature dependence was later remeasured[23] and the binding energy was found to be slightly negative, i.e., O_4^* is not bound. At the same time, the absolute emission intensity of the 6340 A band was measured; its radiative half-life was found to be about 25 msec.[23] Some experiments done by Schiff et al[18] indicated that the 6340 A emission intensity was directly proportional to the $O_2(^1\Delta_g)$ concentration, a result which does not agree with the quadratic relationships found in the work of Ogryzlo et al.,[7,23] and in subsequent investigations[13,24] including this work.

The most recent work on the emission reactions and the nature of the O_4^* complex is that of Arnold,[13] who found that the rate constant for the light emitting process was independent of pressure over the range 1-5 torr and was also unaffected by the addition of up to 25% of several non-reacting gases. These results combined with the temperature dependence study are consistent with an O_4^* complex consisting of either a metastable double molecule or simply a colliding pair of molecules. The suggestion was also made[13] that this complex may be the intermediate in both the disproportionation reaction and the chemiluminescent one.

Simultaneous electronic transitions of two O_2 molecules are well known in absorption spectroscopy where bands due to double transitions to both the $^1\Delta_g$ and the $^1\Sigma_g^+$ states have been observed in solid, liquid and gaseous spectra.[25-28] In fact, the blue color of liquid oxygen is mostly derived from these double transitions.[28] The suggestion of some sort of O_4 molecule was first made in 1933 by Ellis and Kneser[25] who

observed the absorption bands in the liquid. Later, Salow and Steiner[26] studied the absorption of compressed O_2 gas, finding that the absorption intensity was dependent on the square of the O_2 pressure and independent of the partial pressure of added gases.

In order to do kinetic studies of the emission spectra, a primary requirement is a good method of measuring excited molecule concentrations. The most satisfactory method of detection of $O_2(^1\Delta_g)$ has been that used by Ogryzlo et al.[23] and by Arnold[13] who used an isothermal calorimetric detector. This is a device which measures the excited molecule concentration by measuring the heat liberated when the molecules are deactivated on a catalytic surface. The (0,0) band of the $(^1\Delta_g \rightarrow {}^3\Sigma_g^-)$ system at 12,680 A has also been used to detect $O_2(^1\Delta_g)$ but it lies in a difficult spectral region and the results obtained by this method have so far been somewhat equivocal.[18]

The present work was undertaken in an attempt to apply the technique of electron paramagnetic resonance (EPR) detection to the study of the $O_2(^1\Delta_g)$ molecule. This method has the advantages, in common with many spectroscopic methods, of excellent selectivity, high sensitivity, and non-destructiveness. The EPR spectra of most simple paramagnetic species are sufficiently distinctive to allow easy and unambiguous identification. The primary disadvantages of the method are its inability to detect non-paramagnetic species and the relatively complex instrumentation and calculation required, particularly for obtaining absolute concentrations. In the study of the O_2 system reported here, the use of EPR is particularly appropriate, since $O_2(^1\Delta_g)$, $O_2(^3\Sigma_g^-)$ and O atoms are all paramagnetic.

II. EPR SPECTRUM OF $O_2(^1\Delta_g)$

The EPR spectrum of $O_2(^1\Delta_g)$ is shown in Fig. 1. The spectrum, consists of four approximately equally spaced lines about 100 gauss apart, with intensity ratios of about 2:3:3:2. Linewidths are about 1.5 gauss at 0.5 torr, similar to the linewidths observed for $O_2(^3\Sigma_g^-)$ resonances. The experimental g-values for each of the four lines were accurately measured and are listed in Table I.

How these lines originate can readily be seen from a simple vector model calculation. In Fig. 2 are shown the angular momentum vectors for an $O_2(^1\Delta_g)$ molecule in a magnetic field. The angular momentum of rotation of the nuclei is $\bar{N}$, $\bar{\Lambda}$ is the electronic orbital angular momentum, and $\bar{J}$ is the total angular momentum. There is no spin angular momentum, of course, because we are dealing with a singlet state and the nuclear spin of O^{16} is zero. The Z-axis is chosen to be parallel to the direction of the magnetic field, $\bar{H}$, and M_J is the projection of $\bar{J}$ onto this axis.

The energy which the molecule has due to the interaction of the magnetic field with the molecular moment ($\bar{\mu}$) is just

$$E = -\bar{\mu} \cdot \bar{H} \tag{3}$$

The magnetic moment of the molecule lies along $\bar{\Lambda}$ and is equal to

$$\bar{\mu} = g_L \beta \bar{\Lambda} \tag{4}$$

where β is the Bohr magneton and g_L is the spectroscopic splitting factor, which in this case is very nearly equal to -1.0 since only orbital angular momentum is involved. The average component of $\bar{\mu}$

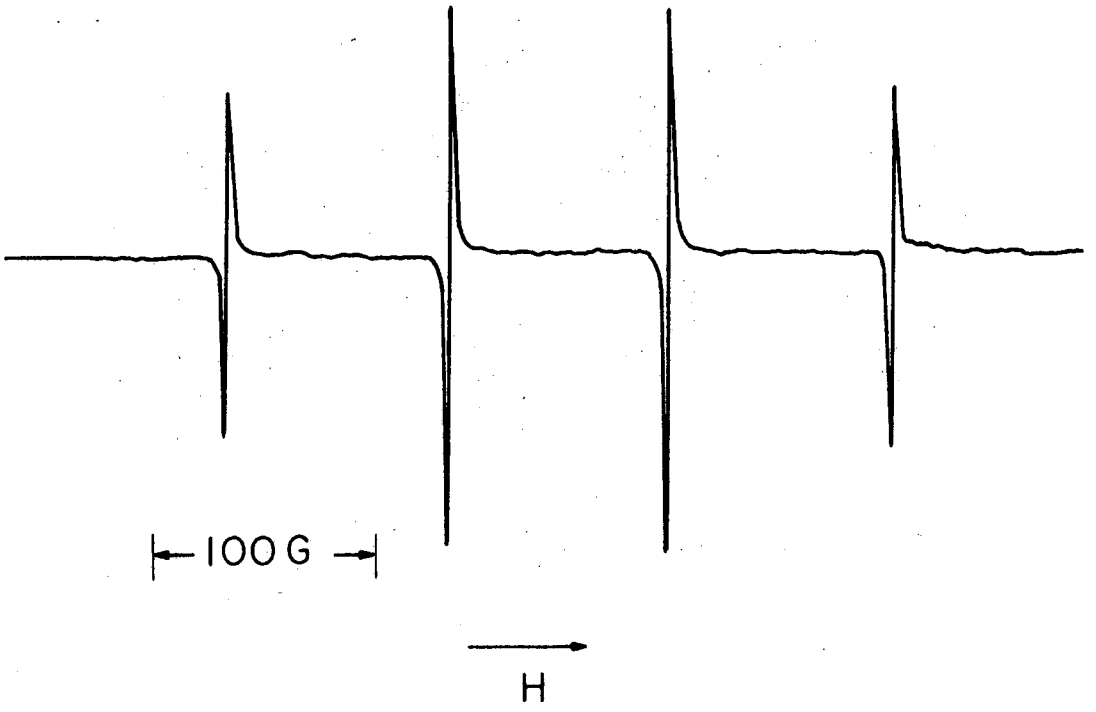

XBL675-3005

Fig. 1 EPR spectrum of $O_2(^1\Delta_g)$.

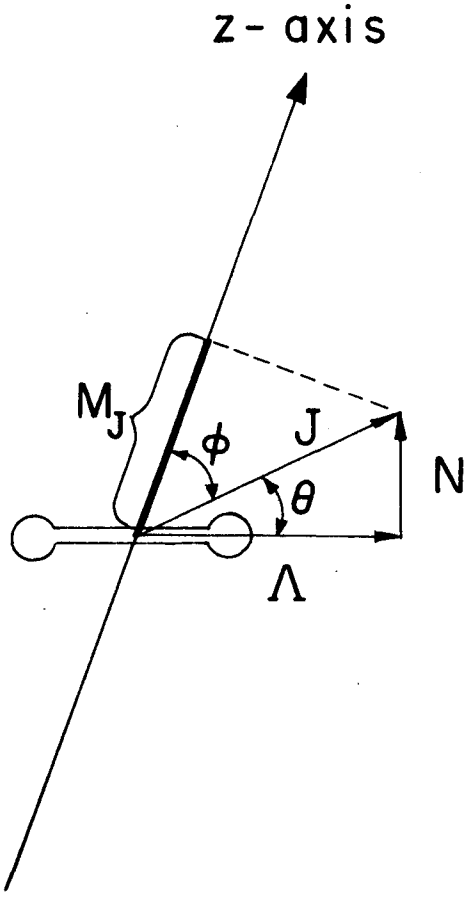

XBL675-3006

Fig. 2 Vector diagram of an $O_2(^1\Delta_g)$ molecule in a magnetic field parallel to the Z-axis.

Table I.

The observed spectrum for $^1\Delta_g$ O_2.

Transition M_J	Field (gauss)	$h\nu/\mu_o H$ obs.(a)	$h\nu/\mu_o H$ cal.(b)
-2 → -1	10,090.3	0.65596	0.65598
-1 → 0	9,988.7	0.66264	0.66265
0 → 1	9,885.6	0.66956	0.66955
1 → 2	9,781.4	0.67670	0.67668

(a) $\mu_o/h = 13.9960 \times 10^5$ $G^{-1} sec^{-1}$.

(b) With $g_J = -0.66662$ and assuming $B_o = 1.4178$ cm^{-1} (see ref. 11).

in the Z direction (μ_Z) is conveniently calculated by first projecting it onto $\bar{J}$ to get μ_J which can then be projected directly onto the Z-axis:

$$\mu_J = \mu \cos\theta = \mu \frac{\Lambda}{\sqrt{J(J+1)}} \tag{5}$$

$$\mu_Z = \mu_J \cos\phi = \mu \frac{\Lambda M_J}{J(J+1)} = \frac{\beta \Lambda^2 M_J}{J(J+1)} \tag{6}$$

where we have assumed $g_L = -1.0$.

The selection rule for EPR transitions is $\Delta M_J = \pm 1$, which gives,

$$\Delta E = \frac{\Lambda^2 \beta H}{J(J+1)} = g_J \beta H \tag{7}$$

where g_J is the experimental g-value. For $O_2(^1\Delta_g)$, $\Lambda = 2$; thus the lowest possible J value is 2, for which $g_J = 2/3$. At a frequency of 10 gHz (X-band) this corresponds to a field of about 10,000 gauss. For $J = 3$, $g_J = 1/3$, so that a magnetic field of 20,000 gauss would be required to detect the transitions at this frequency. As we were unable to produce a field this large with our magnet, no $J = 3$ or higher transitions were observed; however, the $J = 3$ transitions would appear at a lower field with a lower frequency spectrometer, for example, S-band. Work on this is in progress in this laboratory.

Using the vector model described above, we predict the energy levels shown in the center column of Fig. 3, which would result in an EPR spectrum for the $J = 2$ transitions consisting of only a single 4-fold degenerate line. In order to explain the observed quartet one needs to employ somewhat more sophisticated methods, such as second order perturbation theory.

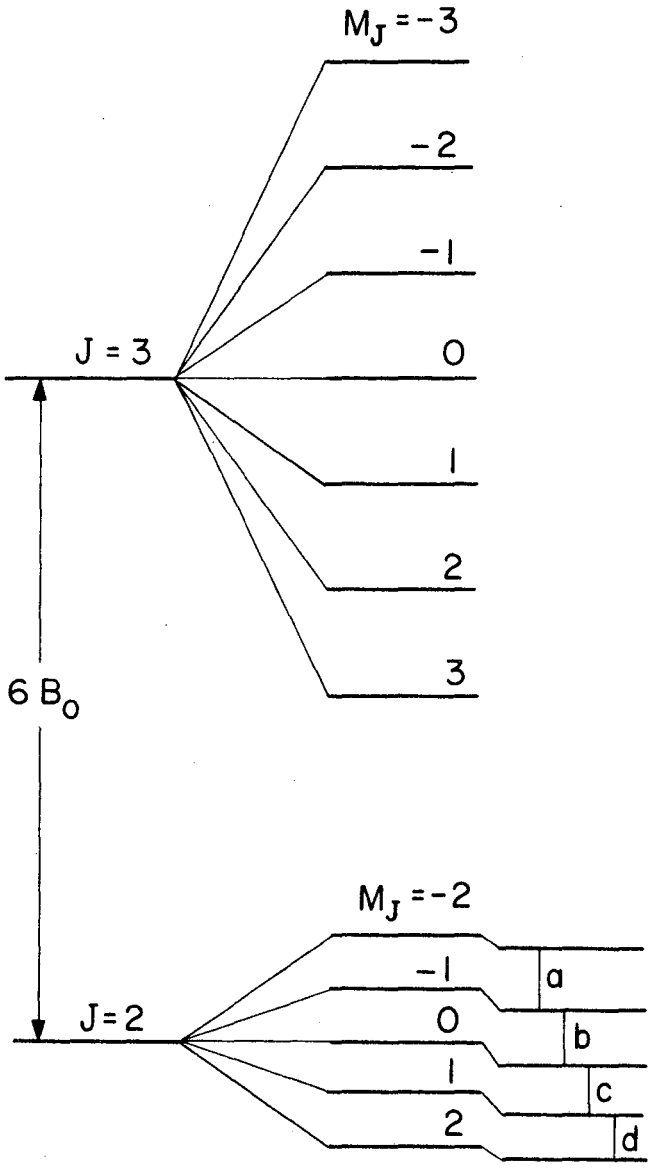

XBL675-3007

Fig. 3 $O_2(^1\Delta_g)$ energy levels in a magnetic field.

The Hamiltonian for the molecule in a magnetic field can be written

$$\mathcal{H} = H_o - \bar{\mu} \cdot \bar{H} \tag{8}$$

where H_o is the Hamiltonian in the absence of the field. To use perturbation theory, we let $H' = -\bar{\mu} \cdot \bar{H}$ and use the representation in which J^2, Λ, and M_J are diagonal. The first order correction to the energy will be:[29]

$$E' = (J, \Lambda, M_J \,|H'|\, J, \Lambda, M_J) \tag{9}$$

We can express H' in terms of a direction cosine as

$$H' = -\mu H \cos \Phi_{Zz} \tag{10}$$

where Φ_{Zz} is the angle between the space fixed Z-axis (parallel to H) and the molecule-fixed z-axis (parallel to $\bar{\mu}$). The matrix element in Eq. (9) then becomes

$$E' = -\mu H(J, \Lambda, M_J \,|\cos \Phi_{Zz}|\, J, \Lambda, M_J). \tag{11}$$

The direction cosines and their matrix elements have been discussed and conveniently tabulated by Strandberg.[30] From the tabulation one finds that

$$(J, \Lambda, M_J \,|\cos \Phi_{Zz}|\, J, \Lambda, M_J) = -\frac{\Lambda M_J}{J(J+1)} \tag{12}$$

so that

$$E = E_o + \frac{\Lambda^2 M_J}{J(J+1)} g_L \beta H \tag{13}$$

The zero order energy E_o is just the energy for a symmetric top,[10]

$$E_o = B_o [J(J+1) - \Lambda^2] \tag{14}$$

Up to this point the results are identical with the vector model calculation. We now calculate the second order correction to the energy E'', which takes into account the interaction of the $J = 2$ and $J = 3$ levels. This term is given by[29]

$$E'' = \frac{(J, \Lambda, M_J|H'|J+1, \Lambda, M_J)(J+1, \Lambda, M_J|H'|J, \Lambda, M_J)}{E_J - E_{J+1}} \tag{15}$$

In order to evaluate E'', we need the direction cosine matrix elements $(J, \Lambda, M_J|\Phi_{Zz}|J+1, \Lambda, M_J)$ and $(J+1, \Lambda, M_J|\Phi_{Zz}|J, \Lambda, M_J)$, which are equal by symmetry. From Strandberg's table[30] one finds

$$(J, \Lambda, M_J|\Phi_{Zz}|J+1, \Lambda, M_J) = \frac{\sqrt{9 - M_J^2}}{3\sqrt{7}} \tag{16}$$

for $J = 2$, $\Lambda = 2$. The total energy to second order for the $J = 2$ levels is then:

$$E = B_o[J(J+1) - \Lambda^2] + g_J\beta H M_J + \frac{M_J^2 - 9}{378B_o} \Lambda^2 g_L^2 \beta^2 H^2 \tag{17}$$

and the energy difference between the M_J and M_{J+1} levels is

$$\Delta E = g_J\beta H - \frac{(2M_J + 1) \Lambda^2 g_L^2 \beta^2 H^2}{378B_o} \tag{18}$$

The resulting energy level diagram is represented on the right side of Fig. 3. The predicted transitions (designated a,b,c, and d) are four roughly equally spaced lines, in good agreement with our observations.

One can, however, predict the transitions still more accurately than this. To do so we diagonalize the 2x2 Hamiltonian matrix for $J = 2$ and $J = 3$ exactly. The Hamiltonian can be written

J	2	3
2	H_{22}	H_{23}
3	H_{23}	H_{33}

(19)

The off-diagonal terms H_{23} are the result of mixing of the $J = 2$ and $J = 3$ levels by the second order Zeeman effect. In the usual fashion[29] we obtain the secular equation

$$(H_{22} - E)(H_{33} - E) - H_{23}^2 = 0 \tag{20}$$

which can be solved for E to give

$$E = \frac{H_{22} + H_{33}}{2} \pm \frac{H_{33} - H_{22}}{2} \left(1 + \frac{4H_{23}^2}{(H_{33} - H_{22})^2}\right)^{1/2} \tag{21}$$

Now let

$$x = \frac{4H_{23}^2}{(H_{33} - H_{22})^2} \tag{22}$$

and expand the root near H_{22} in a Taylor series:

$$E_2 = H_{22} + \frac{H_{33} - H_{22}}{4}\left(-x + \frac{x^2}{4} - \frac{x^3}{8} + \frac{5x^4}{64} - \ldots\right) \tag{23}$$

Using the direction cosine matrix elements which we have calculated

above, H_{22}, H_{33}, and H_{23} are readily evaluated:

$$H_{22} = 2B_o + 2/3\ g_L\beta HM_J \tag{24}$$

$$H_{33} = 8B_o + 1/3\ g_L\beta HM_J \tag{25}$$

$$H_{23} = \frac{2\sqrt{9 - M_J^2}}{3\sqrt{7}}\ g_L\beta H \tag{26}$$

and

$$\chi = \frac{16(9 - M_J^2)\ g_L^2\beta^2H^2}{63[6B_o - \frac{1}{3}\ g_L\beta HM_J]^2} \tag{27}$$

so that

$$E_2 = 2B_o + \frac{2}{3}\ g_L\beta HM_J + \frac{6B_o - \frac{1}{3}\ g_L\beta HM_J}{4}\left(-\chi + \frac{\chi^2}{4} - \frac{\chi^3}{8} \cdots\right)$$

$$= 2B_o + g_J\beta HM_J + \epsilon(M_J) \tag{28}$$

For the transition $M_J \rightarrow M_{J+1}$

$$\Delta E_2 = g_J\beta H + \epsilon(M_J + 1) - \epsilon(M_J) = g_{eff}\beta H \tag{29}$$

where g_{eff} is the experimental g-value.

If a quantity Δg is defined as

$$\Delta g = \frac{\epsilon(M_J + 1) - \epsilon(M_J)}{\beta H} \tag{30}$$

then $g_J = g_{eff} - \Delta g$, and we can calculate g_J from the observed values

of g_{eff} and Eq. (30). This calculation was performed* for each of the four lines giving the values g_J = -0.66660, -0.66661, -0.66663, and -0.66664. The average value of g_J = -0.66662 was then used with Eqs. (28) and (29) to obtain the calculated g-values listed in Table I.

It can be seen that the use of the single adjustable parameter g_J gives a very good fit to the data. There is a small systematic deviation between the calculated and observed values that could be eliminated by using a B_o value which is smaller by 3×10^{-3} cm^{-1} from the spectroscopic value.[11] It is not clear at this time if this correction is justified.

Our assigned g_J value must contain some contribution from the rotational magnetic moment, but with only transitions of a single J value it is not possible to determine g_r. If the g_r value for the $^1\Delta_g$ state is identical to that for the ground $^3\Sigma_g^-$ state[31] then one can obtain a value for g_L = -0.99987. This value differs from -1.0 by about the same amount that the Landé g value for the O-atom ^3P state[32] differs from its simple theoretical value, corrected for the electron spin anomaly. From this fact we can conclude that most of the reduction in the g_L value is due to a diamagnetic correction and not due to rotationally induced mixing with $^1\Sigma$ and $^1\pi$ states.

In order to determine the intensities of each of the four lines, it is necessary to calculate $|(\mu_r)_{ij}|^2$, the average squared matrix element of the component of the magnetic moment in the direction of the microwave magnetic field. Tinkham and Strandberg[33] have shown that for

---

* The computation was performed on an SDS 910 computer by Dr. D.H. Levy.

$M_J = +1$ transitions,

$$|(\mu_r)_{ij}|^2 = 2|(\mu_x)_{ij}|^2 \; f_+ \tag{31}$$

where f_+ is the filling factor. Equation (31) can be evaluated by again making use of the direction cosine matrix elements:

$$|(\mu_x)_{ij}|^2 = \beta^2\Lambda^2(J, \Lambda, M_J \; |\cos\Phi_{Xz}| \; J, \Lambda, M_J + 1)^2 \tag{32}$$

$$= \beta^2\Lambda^2 \left[\frac{\Lambda}{2J(J+1)} \sqrt{(J - M_J)(J + M_J + 1)} \right]^2$$

For $J = 2$, $\Lambda = 2$, this becomes

$$|(\mu_x)_{ij}|^2 = \frac{1}{9}\beta^2(2 - M_J)\,(3 + M_J) \tag{33}$$

so that

$$|(\mu_r)_{ij}|^2 \equiv |\mu_{ij}|^2 = \frac{2}{9} f_+\beta^2(2 - M_J)\,(3 + M_J) \tag{34}$$

In Table II are listed the matrix elements for each of the four transitions, showing the predicted intensity ratios of 2:3:3:2.

Table II.

Transition matrix elements for $O_2(^1\Delta_g)$ $J = 2$ transitions.

Transition	$\lvert\mu_{ij}\rvert^2$
$M_J = -2 \rightarrow -1$	$8/9\; f_+\beta^2$
$-1 \rightarrow 0$	$12/9\; f_+\beta^2$
$0 \rightarrow 1$	$12/9\; f_+\beta^2$
$1 \rightarrow 2$	$8/9\; f_+\beta^2$

III. RATE CONSTANT MEASUREMENTS

A. Experimental

1. Materials

A single tank of Matheson "Extra Dry" grade oxygen (99.6% minimum purity, 0.1% nitrogen maximum, 0.4% argon maximum) was used for all experiments with tank oxygen. Chemically prepared oxygen was produced by thermal decomposition of potassium permanganate. General Dynamics helium (Grade A, 99.995% minimum purity) and argon (99.99% minimum purity) were used for the mixed gas experiments. Nitrogen dioxide (99.5% minimum purity) and ethylene (C.P., 99% minimum purity) were obtained from the Matheson Co.

2. Discharge-Flow System

A diagram of the discharge flow system used is shown in Fig. 4. The gas to be used was placed in the reservoir which consisted of two 35 l stainless steel tanks which could be connected to form a 70 l reservoir or used singly. The reservoir was filled to a pressure of about one atmosphere. In some cases when pure O_2 prepared from $KMnO_4$ was used, a sample flask of the liquified gas placed in a liquid oxygen bath was used as the reservoir. After leaving the reservoir, the gas passed over a small amount of degassed distilled water contained in a trap at -10°C. The water vapor thus added to the stream insured the removal of any excited $O_2(^1\Sigma_g)$[13] and also appeared to increase the yield of $O_2(^1\Delta_g)$ by 20 or 30%. The flow rate was measured with a calibrated Brooks Rotameter flowmeter and controlled with a Nupro 1/4" stainless steel fine metering valve.

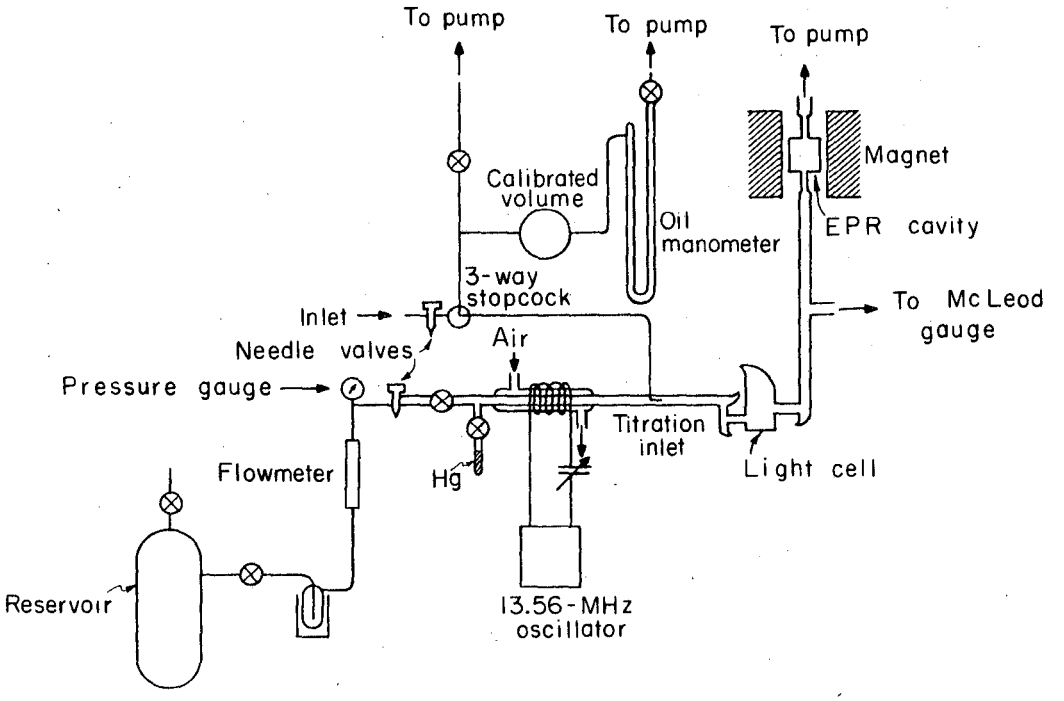

Fig. 4 The discharge-flow system.

The gas flow passed by a small sidearm which contained mercury and then into the discharge tube, which was a 30 cm long air cooled quartz condenser. Several turns of heavy Formvar insulated copper wire were wrapped around the outside of the condenser. This coil was connected in series with a tuning capacitor and the circuit was powered with a 200 w radio-frequency (13.56 MHz) diathermy unit. It was found that the spreading of the discharge plasma could be reduced by using a grounded copper sleeve which was placed around the discharge tube adjacent to the downstream end of the coil.

A separate inlet system was used to feed gas to the small titration inlet located 19 cm downstream from the end of the discharge tube. Gas entered through a 1/8" stainless Nupro very fine metering valve. By means of a 3-way stopcock the gas could either be sent directly to the titration inlet or to the flowmeter section, which consisted of a calibrated volume connected to an oil manometer containing Dow-Corning No. 704 silicone fluid. When it was desired to measure a steady flow entering the needle valve and going to the titration inlet, the flow was diverted into the calibrated volume for a timed interval and the pressure rise was measured. As long as the pressure in the flowmeter volume was very much smaller than the (constant) pressure on the external side of the needle valve, the flow through the valve remained constant.

After passing by the titration inlet the main gas stream flowed through an additional 21 cm of tubing and two light traps, and entered the light cell. This cell had a two-inch diameter flat pyrex end window and was shaped as shown in Fig. 4 so as to be reflectionless.

The volume of the cell was 125 cm^3. Gas leaving the cell passed through another light trap and 55 cm of tubing on its way to the EPR cavity. All three light traps, the light cell, and the tubing connecting them were painted with several coats of opaque flat black paint. All tubing between the discharge and the EPR cell entrance tube was 15 mm i.d. pyrex, except for short connecting sections of 15 mm i.d. quartz and quartz-pyrex seals adjacent to the discharge tube and EPR cell. The entrance to the EPR cell was through a 5.5 cm section of 10 mm i.d. quartz tubing; the cell itself consisted of a quartz pillbox with a volume of 42 cm^3 (see Fig. 9). The gas exited past a 5 liter ballast bulb to maintain uniform flow and was pumped out through a trap at -196°C with a Kinney KC-8 mechanical pump.

Under normal conditions, a large number of oxygen atoms were formed in the discharge. It was desirable to eliminate as many of these as possible in order to prevent interference due to the emission of light from the reaction $O + NO = NO_2 + h\nu$. The emission is a broad continuum which reaches a maximum near the 6340 A band.[34] The NO is formed in the discharge from small amounts of nitrogen contained in the oxygen as an impurity. When no mercury was present, the NO-O glow was sufficiently intense that it was easily visible in a darkened room when tank oxygen was flowed through the discharge at 0.5 torr. No visible glow was produced when oxygen prepared from $KMnO_4$ was used.

Oxygen atoms were removed by a method similar to that used by Ogryzlo[23] and others.[13,18] The stopcock on the sidearm containing Hg at 25°C was always left open so a small amount of mercury vapor was continually being added to the gas stream. In addition, a temporary discharge was excited at a point between the main discharge tube and

the titration inlet. With the main discharge not operating, this secondary discharge was excited for about an hour during which time O_2 was flowed through the system and the mercury in the sidearm was heated strongly. The resulting brownish film (presumably HgO) deposited just downstream from the end of the main discharge reduced the O atom concentration considerably without seeming to affect the $O_2(^1\Delta_g)$ concentration. The system had been in previous contact with mercury vapor so it was not possible to observe the enhancement effect noted by March, Furnival and Schiff.[18] The remaining O atom concentration was roughly measured with the EPR spectrometer and was found to be about 10^{10} atoms/cm^3 at a moderately high discharge power level and a pressure of 0.5 torr. The atom concentration was observed to be strongly dependent on the power level. It was also found that the HgO film could be easily removed for photomultiplier calibration purposes by exposing it to NO or discharged NO_2.

In order to measure the pressure in the EPR cavity accurately, it was necessary to correct for the pressure drop between the point at which the McLeod gauge was connected and the cavity. This pressure difference was determined by making use of the dependence of $O_2(^3\Sigma_g^-)$ EPR linewidths on pressure. The width of one of these lines was measured as a function of pressure both under the usual flow conditions and under static conditions. These results gave a measure of Δp, the difference between the static and dynamic pressure readings corresponding to the same linewidth, as a function of pressure. From Poiseulle's equation[35] for a system undergoing viscous flow we have

$$\Delta p = (\text{const}) \frac{F}{\bar{p}} \qquad (35)$$

where F is the mass flow rate, (e.g., molecules/sec) and $\bar{p}$ is the average system pressure. The "constant" factor contains geometrical parameters, universal constants, the temperature and viscosity. Letting p_m represent the pressure measured under flow conditions, it is easily seen that if Δp is small, $\bar{p} \simeq p_m$, and a graph of Δp vs p_m will have the same shape as the F/p_m vs p_m curve for our system. The latter curve was measured and could be satisfactorily fitted to the Δp vs p_m data. In Fig. 5, the plotted points were determined from the linewidth vs pressure curves and the solid line is the measured F/p_m vs p_m curve whose vertical axis has been scaled to give the best fit to the points.

The magnitude of the correction is about 10%. The viscosities of any two of the gases used in these experiments do not differ by more than 10% so the same corrections were applied for all mixtures.

3. Photomultiplier System

Figure 6 is a diagram of the experimental arrangement used to measure the emission from the gas in the light cell. In order to prevent any light from being piped through the pyrex walls of the light cell, a narrow annular mask was used to cover the edge of the cell window. A 2" diameter interference filter with a center frequency of 6200 A and a width at half maximum of 400 A was placed in front of the cell window. A 24" long light pipe was constructed from a 2" diameter Lucite rod whose ends were squared and polished. The rod was then wrapped with a layer of aluminum foil and a covering of black polyethylene film. The light pipe was used to enable the photomultiplier to be operated at a greater distance from the EPR magnet, since

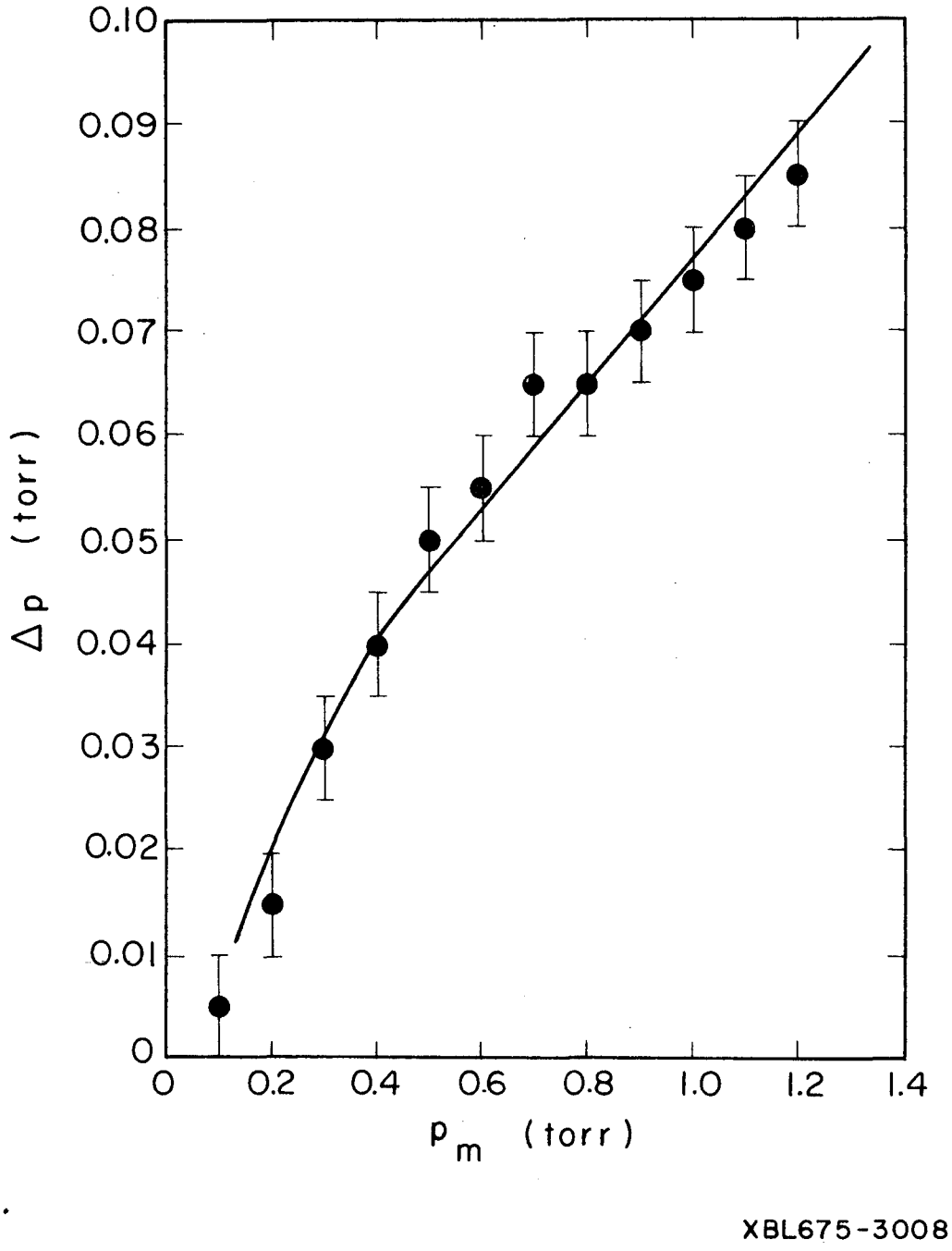

Fig. 5 Pressure drop correction (Δp) as a function of measured pressure (p_m).

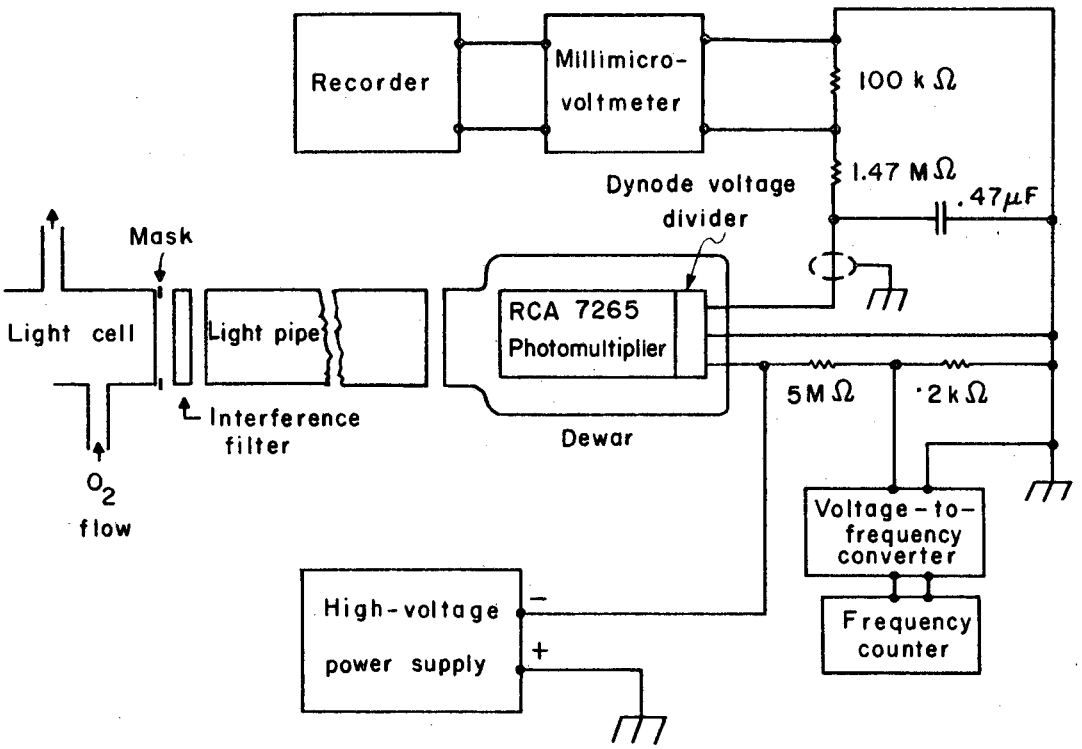

Fig. 6 The emission detection system.

its sensitivity was strongly affected by stray magnetic fields. Even when the light pipe was used, the effect of raising or lowering the magnetic field could be easily seen on the photomultiplier output. In order to eliminate errors from this source all light measurements were made with the magnet set to the $O_2(^1\Delta_g)$ $M_J = 0 \rightarrow 1$ transition.

A liquid nitrogen cooled RCA 7265 photomultiplier tube was used to detect the light emission which entered the photomultiplier Dewar from the light pipe through a 2" diameter pyrex window. The tube has an S-20 response, which means that its sensitivity at 6340 A is nearly 50% of its maximum sensitivity which occurs at 4200 A. The photomultiplier output was measured across a precision 100 KΩ resistor in series with a 1.47 MΩ precision resistor. A 0.47 μF capacitor was placed in parallel with the resistors to give a response time constant of about 0.8 sec. The voltage across the 100 KΩ resistor was measured with a Keithley model 149 Milli-microvoltmeter which was used to drive a Brown 50 mV chart recorder. The photomultiplier current was never allowed to exceed 1 μa.

The high voltage supplying the dynode voltage divider was continuously monitored with a Vidar 100 kHz voltage-to-frequency converter and a Hewlett-Packard frequency counter. It was frequently convenient to change the photomultiplier sensitivity by changing this voltage. This method allowed the sensitivity to be varied over a very wide range while permitting the Milli-microvoltmeter to be operated at low sensitivity, which reduced pickup from the discharge. The relative sensitivity of the photomultiplier at different supply voltages was determined by measuring the signal from a steady light source at several

pairs of voltages. The calibration obtained is shown in Fig. 7. In this figure we have listed the voltage steps used along the abcissa. These voltages are the ones measured with the counter and must be multiplied by 2500 to give the true supply voltages. The ordinate represents the photomultiplier signal at the lower voltage divided by the signal at the higher voltage. The points plotted are averages of several measurements. Only the voltages listed were used and the sensitivity ratios were reproducible to within at least 1%.

The lightproofing of the light cell was checked by measuring the photomultiplier signal with the discharge excited but with no gas flowing. The signal was identical with that obtained when the discharge power was off, after subtracting the small signal due to pickup from the discharge. The pickup signal was measured by simply turning off the photomultiplier high voltage supply.

In order to make certain that the photomultiplier gain did not change significantly between experiments, a constant light source was used. It consisted of a small 24 V tungsten filament bulb which was fixed in place to shine through a small hole in a metal plate at the side of the photomultiplier Dewar just behind the entrance window. The bulb was operated from a constant current source at 102.10±0.05 ma, about one-fourth of its rated current. Day to day variations in the photomultiplier sensitivity, after an hour or so of warm up, seldom exceeded 3 or 4% and were never more than 10%. In a few runs a small correction was made to account for these changes.

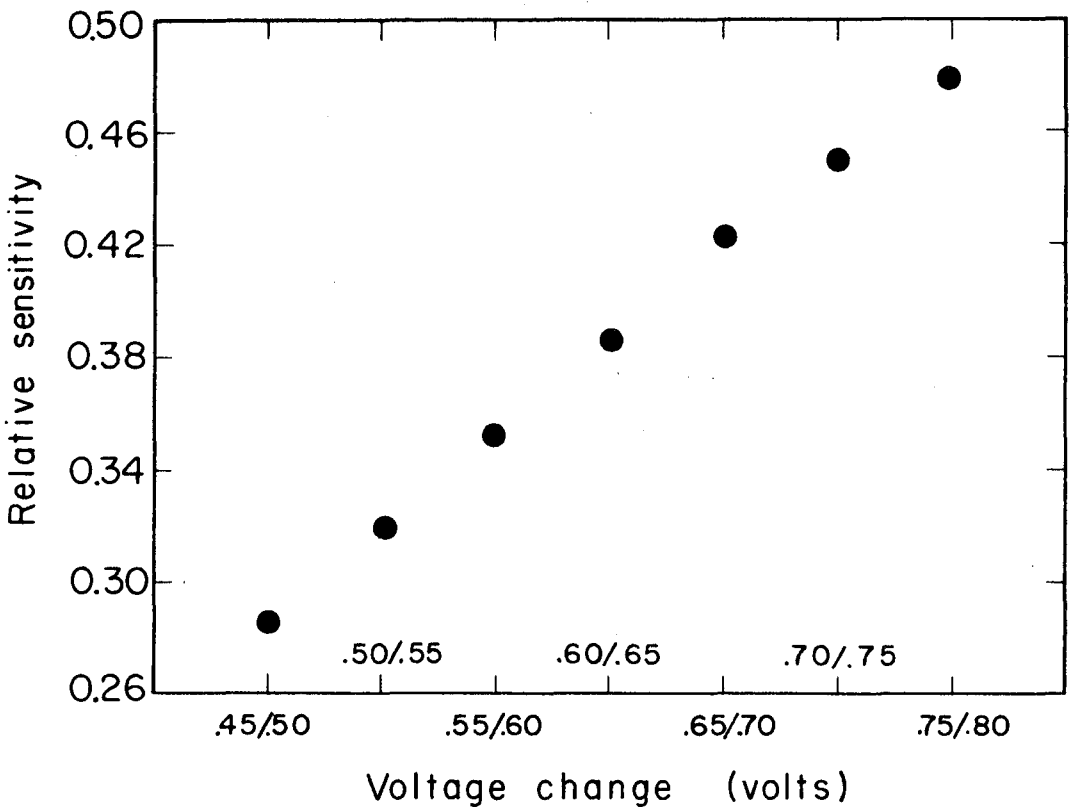

XBL675-3011

Fig. 7 Photomultiplier relative sensitivity calibration.

a. Measurement of absolute sensitivity of photomultiplier system. In order to determine the absolute sensitivity of the light detection system, the reaction

$$O + NO = NO_2 + h\nu \tag{36}$$

was used as a standard. The emission intensity from this reaction is proportional to (O)(NO) over a fairly wide pressure range, and the absolute quantum yield has been measured.[34,36] The overall rate constant for emission over the region 3875-14000 A is given as 6.4×10^{-17} cm^3/molecule-sec at 300°K.[34] Since we employed an interference filter in this work, the fraction of the total emission intensity which was actually detectable was

$$F_1 = \frac{\int I_{NO}(\lambda)T(\lambda)d\lambda}{\int I_{NO}(\lambda)d\lambda} \tag{37}$$

where $I_{NO}(\lambda)$ is the intensity of the NO-O emission as a function of wavelength λ and $T(\lambda)$ is the fractional transmittance of the interference filter used. The value of the numerator was calculated graphically using the data of Fontijn, Meyer and Schiff[34] and data supplied by the manufacturer of the interference filter. The value of the denominator is also given by Schiff, et al.[34] The resulting value of F_1 was 5.8×10^{-2}, which gives an effective rate constant of $k_{NO} = 3.7\times10^{-18}$ cm^3/molecule-sec for the NO-O emission detected in our system.

Similarly, to measure the rate of emission from $O_2(^1\Delta_g)$ in the 6340 A band, it is necessary to multiply the measured intensity by the factor

$$F_2 = \frac{\int I(\lambda)d\lambda}{\int I(\lambda)T(\lambda)d\lambda} \qquad (38)$$

where $I(\lambda)$ is the intensity of the emission band centered around 6340 A as a function of wavelength. This factor accounts for the fact that our system sees only a part of the total emission from this band. The integrals were calculated graphically using the emission spectrum measured by Bader and Ogryzlo,[7] giving the result $F_2 = 1.89$.

The calibration was performed by adding a small, constant flow of NO_2 to the main flow by means of the titration inlet immediately after the discharge. The main flow consisted of a constant stream of partially dissociated oxygen. The reaction

$$O + NO_2 = NO + O_2 \qquad (39)$$

is very fast[1] and all of the NO_2 was converted to NO within a very short distance past the inlet. The reaction of NO with O is relatively slow[1] and any NO_2 produced this way would immediately be reconverted to NO by reaction (39). The amount of NO present downstream was therefore exactly equal to the amount of NO_2 added at the inlet as long as this amount did not exceed the initial O atom concentration.

The oxygen atom concentration was determined by titrating with NO_2.[1] The visible NO-O glow just disappeared when the NO_2 flow was equal to the O atom flow. This gave a measure of the initial (no NO_2 flowing in) O atom concentration at a point just past the titration inlet. The concentration of atoms when a small amount of NO_2 was being added was then equal to the difference between the initial O atom concentration and the amount of NO_2 added.

Between the titration port and the light cell was about 19 cm of 15 mm i.d. pyrex tubing, and it was necessary to correct for the loss of atoms while passing through this section. The average time required for an atom to travel from the titration port to a point halfway through the light cell was about 0.18 sec under the flow conditions used. Atom losses could occur either by recombination at the wall or by the homogeneous processes:

$$\begin{aligned} O + O_2 + O_2 &= O_3 + O_2 \\ O_3 + O &= 2O_2 \end{aligned} \qquad (40)$$

and

$$O + NO + O_2 = NO_2 + O_2 \quad \text{(non-radiative)} \qquad (41)$$

The approximate overall rate constants for these reactions are $k_{40} = 4\times10^{-34}$ cm^6/molecule^2-sec,[1] and $k_{41} = 7\times10^{-32}$ cm^6/molecule^2-sec.[1] (The rate of the non-radiative O + NO reaction is about 600 times faster than the radiative one.)[49] Using the concentrations given in Table III, it is easily verified that losses by either of these processes were only about 1%.

Wall recombination, however, was not insignificant. The recombination coefficient could be estimated from the difference between the O atom concentration at the titration inlet (measured by titration) and the concentration in the EPR cavity (measured by EPR). About half of the atoms were lost between these two points, as can be seen from the upper two rows of Table III. The fact that the fractional loss seems to be independent of concentration indicates that the main loss is first

Table III.

Summary of absolute photomultiplier calibration measurements.

NO_2 flow (cm^3/sec at 1 atm)	(NO) (molecules/cm^3)	(O) at titration port (atoms/cm^3)	(O) at EPR cavity (atoms/cm^3)
0	0	1.50×10^{14}	7.4×10^{13}
2.16×10^{-3}	9.7×10^{13}	5.3×10^{13}	2.5×10^{13}
3.32×10^{-3}	1.50×10^{13}	~0	~0

O_2 flow = 0.313 cm^3/sec at 1 atm.

total pressure = 0.44 torr.

$k_{NO}(NO)(O) = (3.7 \times 10^{-18})(9.7 \times 10^{13})(5.3 \times 10^{13})(0.87)$

$= 1.66 \times 10^{10}$ photons/sec-cm^3.

order with respect to O. The wall recombination coefficient measured in this way was 4.5×10^{-5}, which falls well within the spread of other reported values for pyrex.[1] Using this value, the loss of O atoms between the titration port and the light cell amounted to 13%. The amount of detectable radiation emitted during the calibration (the second row of Table III) was then 1.66×10^{10} photons/sec-cm^3.

4. EPR Measurements

a. Spectrometer and cavity. The spectrometer used was a conventional X-band reflection type with 100 kHz magnetic field modulation and phase detection. The dc magnetic field was produced with a Pacific Electric Motors electromagnet with 12" pole pieces and a 2-5/8" gap. The details

of the spectrometer and magnet have been previously described[37,38] with the exception of those mentioned below. A block diagram of the instrument is shown in Fig. 8.

For some experiments it was necessary to integrate the signal from the phase detector. This was accomplished by first amplifying the phase detector output by a factor of 30 with a Sanborn 8875A differential dc amplifier, and then feeding the amplified signal into a Tektronix Type O (operational amplifier) oscilloscope plug-in unit which was set with a one second time constant. The integrator output, after being attenuated by a factor of 5000, was measured with a Keithley model 149 Milli-microvoltmeter and recorded with a Brown 50 mV chart recorder. The main function of the Milli-microvoltmeter was to serve as a convenient scaler and zero-offset device. The stability of the integrator system was considerably greater than the stability of the phase detector output zero level, even at low spectrometer gain. Usually the doubly integrated signal was the quantity in which we were interested, so the integrator traces were integrated again manually with a planimeter.

For the experiments in which concentration measurements were made, the cavity used was a Varian V-4533 cylindrical cavity which operated in the TE_{011} mode and had an unloaded frequency of about 9.5 GHz. The cavity was disassembled and a quartz pillbox was built to fill the entire volume of the cavity which was then reassembled around the quartz, as shown in Fig. 9. The outer dimensions of the pillbox were 40 mm diameter by 39 mm high, while the dimensions of the cavity into which it was fitted were 41.5 mm diameter by 41 mm high. The inlet and exit tubes were 11 mm o.d. quartz, the outlet terminating in a ball joint.

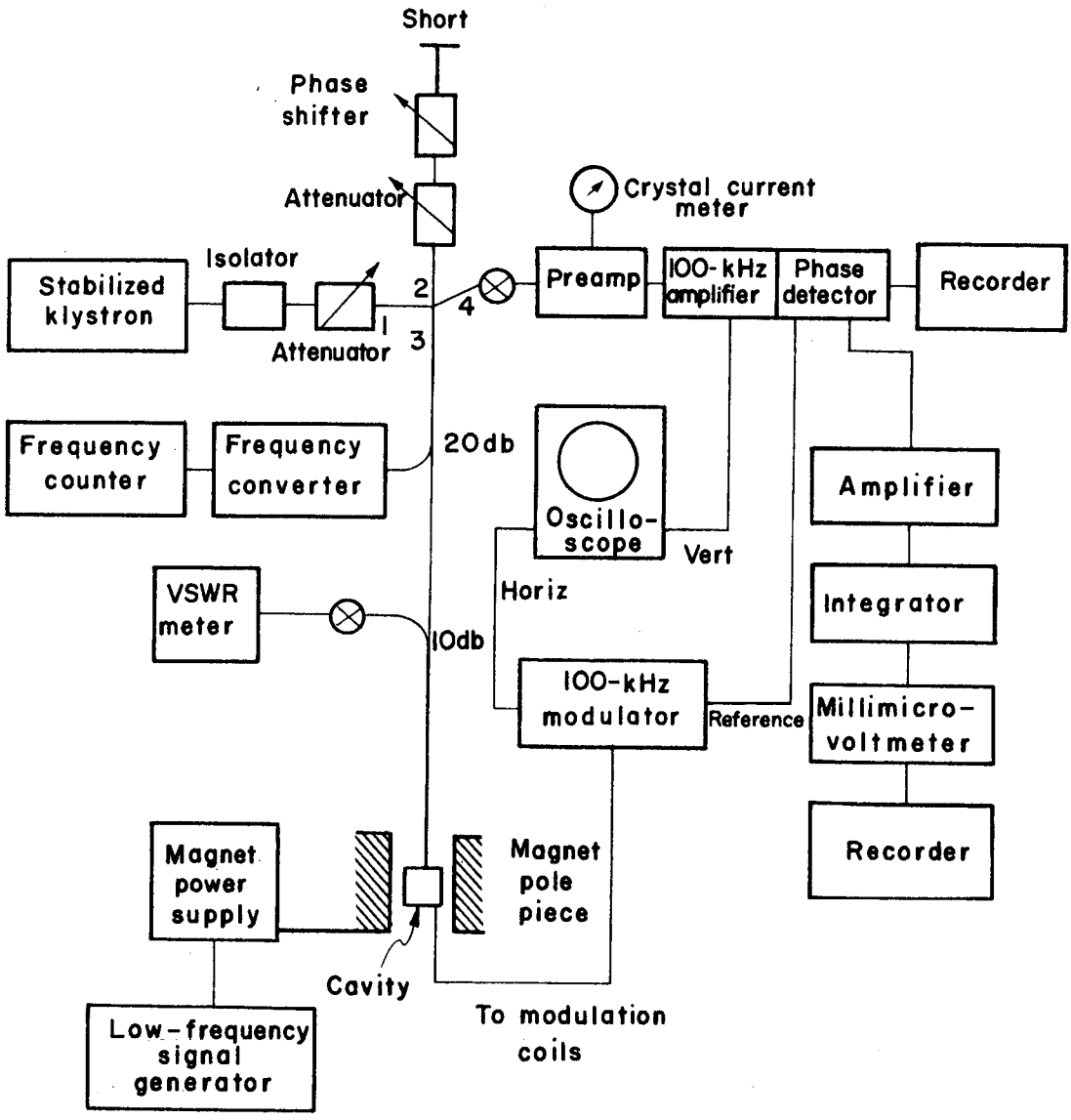

Fig. 8 Block diagram of the X-band EPR spectrometer.

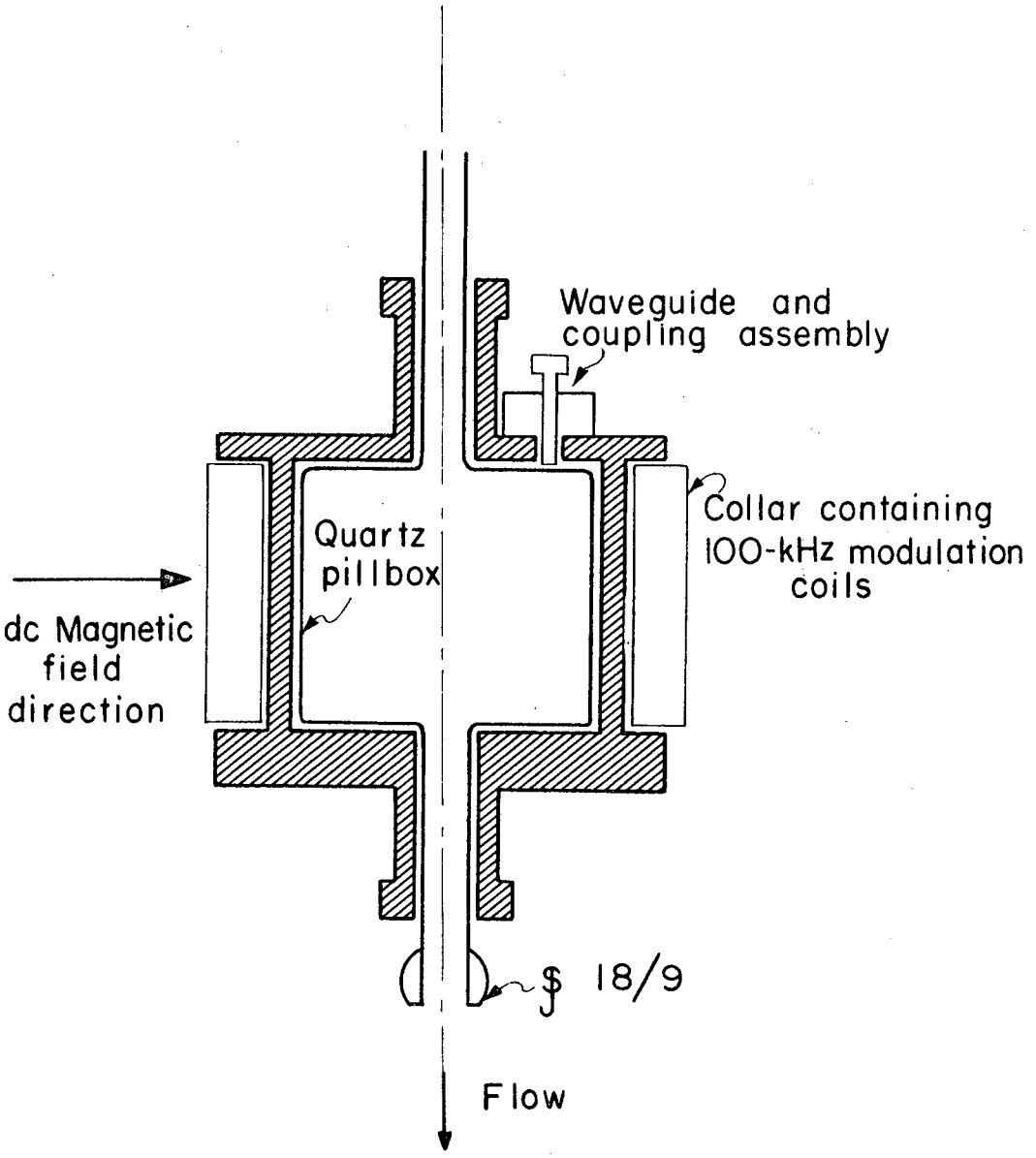

Fig. 9 EPR cavity and quartz pillbox.

The completed assembly had a resonant frequency of 9.29 GHz and a Q of 8,000 to 10,000.

A slightly different arrangement was used for the g-value measurements. A Varian V-4531 rectangular cavity operating in the TE_{012} mode was employed. The discharged oxygen flowed through an 11 mm o.d. straight quartz tube running through the center of the cavity. Magnetic field intensity was measured with a Harvey-Wells NMR Precision Gaussmeter by setting the magnetic field to the center of the EPR line and then tuning the NMR oscillator to the middle of the proton resonance. The NMR frequency was counted directly with a Hewlett-Packard frequency counter. The klystron frequency was measured with a Hewlett-Packard frequency converter and the frequency counter.

A small systematic error in magnetic field measurements was introduced because the NMR probe had to be placed in the magnet gap alongside the cavity, which meant that the probe was directly against one of the pole faces while the gas sample was nearly in the center of the gap. The difference in magnetic field between these two points was measured with the cavity removed and found to be 1.1 ± 0.1 gauss at a total field of 10,000 gauss. The field measurements in Table I have been corrected for this deviation, which was the source of the largest uncertainty in the g-value measurements.

b. Concentration measurements. In order to make absolute concentration measurements with the spectrometer it was necessary to have a convenient standard sample. Ground state O_2 was the obvious choice, as it was always present and, being a gas, filled the cavity in exactly the same way as the excited species and oxygen atoms. Many of the ground state

EPR lines have been carefully measured and calculated by Tinkham and Strandberg.[33]

For this work, we used two of these O_2 lines as calibration standards: line "A", which arises from the transition K = 3, J = 4, M = 3 → 4; and line "C", which corresponds to K = 1, J = 1, M = -1 → 0.[33] Our designations "A" and "C" have no special significance except that C is the same identifying letter used for this line by Westenberg and deHaas,[39] whose work is mentioned below. These two lines appeared at about 9460 (line A) and 5490 G (line C) with the cylindrical cavity Line C was used exclusively for the O atom calibration and line A was only used for the $O_2(^1\Delta_g)$ calibration. For all of the quantitative work with $O_2(^1\Delta_g)$, the line corresponding to the $M_J = 0 \rightarrow 1$ transition was used, which occurred at about 9920 G with the cylindrical cavity.

For a single, unsaturated EPR transition ($i \rightarrow j$), the power absorbed by the sample will be proportional to the imaginary part of the complex susceptibility, χ''_{ij}.[40] The usual derivation[41] gives:

$$\chi''_{ij}(\omega) = \frac{N\omega}{kTZ} e^{-E_i/kT} |\mu_{ij}|^2 F(\omega-\omega_o) \qquad (42)$$

where ω is the angular frequency of the incident radiation, ω_o is the frequency at resonance, N is the number density of absorbing molecules, k is the Boltzmann constant, T is the absolute temperature, Z is the partition function for the species involved, E_i is the energy of the lower state of the transition, and μ_{ij} is the transition matrix element in the direction of the microwave magnetic field. The function $F(\omega-\omega_o)$ is an empirical function which depends on the line shape, which is usually Lorentzian in liquids and gases. It is always normalized so that

$$\int_0^\infty F\,(\omega-\omega_o)\,d\omega = 1 \qquad (43)$$

Since we are using a fixed frequency and varying the magnetic field, it is useful to replace the variable ω with the slowly varying magnetic field, H. The transformation is easily accomplished[42] by using the relation

$$\omega = \omega_o + \frac{d\omega}{dH}\,(H - H_o) \qquad (44)$$

where H_o is the field at which resonance occurs with incident radiation of frequency $\omega = \omega_o$. This equation will be valid for small values of $H-H_o$, i.e., the region close to resonance. From the differential form of the general EPR resonance relation

$$\hbar d\omega = g_{eff}\beta dH \qquad (45)$$

it is seen that $d\omega/dH = g_{eff}\beta/\hbar$ will be independent of H at a fixed frequency. Here, $\hbar$ is Planck's constant divided by 2π, β is the Bohr magneton; and g_{eff}, the effective g-value for the transition of interest, is defined by Eq. (45). For the case of atoms, g_{eff} is simply the Landé g-factor.

Substitution into the normalization equation (Eq. 43),

$$\int_0^\infty F\left(\frac{d\omega}{dH}(H-H_o)\right)\frac{d\omega}{dH}\,dH = 1 \qquad (46)$$

shows that the normalized lineshape function in terms of H is

$$f(H-H_o) \equiv \frac{d\omega}{dH}F\left(\frac{d\omega}{dH}(H-H_o)\right) = \frac{g_{eff}\beta}{\hbar}\,f(\omega-\omega_o) \qquad (47)$$

The absorption is thus proportional to

$$\chi''_{ij}(H) = \frac{N\omega_o\hbar}{kTg_{eff}\beta}\,\frac{\exp(-E_i/kT)}{Z}\,|\mu_{ij}|^2\,f(H-H_o). \qquad (48)$$

The integrated intensity for this transition is defined as

$$I = \int_0^\infty \chi''_{ij}(H)\,dH \qquad (49)$$

so the concentration of absorbing species will be equal to

$$N = \frac{kT\,g_{eff}\beta IZ}{\nu_o h}\,\frac{\exp(E_i/kT)}{|\mu_{ij}|^2} \qquad (50)$$

where ω_o has been replaced by $2\pi\nu_o$. We note that the integrated intensity will be independent of the functional form of $f(H-H_o)$ and hence the line shape, and will be proportional to N.

Tinkham and Strandberg[33] showed that

$$|\mu_{ij}|^2 = \frac{1}{2}(g_{el}^2\beta^2 f_+)\,[4|S_x|_{ij}^2] \qquad (51)$$

where $g_{el} = 2.0023$ is the electronic g-factor, f_+ is the cavity filling factor, and the quantity in brackets is a calculated matrix element. If we define p as[39]

$$p = [4|S_x|_{ij}^2] \exp(-E_i/kT) \tag{52}$$

we get

$$N_\Sigma = \frac{g_\Sigma Z_\Sigma}{g_{el}^2 p} \left(\frac{2kT}{h\nu_o \beta f_+} \right) I_\Sigma \tag{53}$$

The subscript Σ indicates that the quantities refer to a line of the ground ($^3\Sigma_g^-$) state of O_2; g_Σ is just g_{eff} for this line.

The partition function for $O_2(^3\Sigma_g^-)$ is

$$Z_\Sigma = 3 \cdot \frac{kT}{hB} \cdot \frac{1}{2} \tag{54}$$

where B is the rotational constant. The partition function is the product of the electronic spin degeneracy,[3] the high temperature approximation to the rotational partition function, and a factor (1/2) to account for the fact that rotational states with even rotational quantum number (J) are forbidden.[43] This occurs because the electronic wave function for Σ^- states changes sign when the nuclei are permuted. The nuclear spin function must be symmetric for this permutation since O^{16} has no nuclear spin. The total wave function must be symmetric, and since the vibrational and translational partition functions are always symmetric, the rotational partition function must be anti-symmetric. This is true only for odd numbered rotational states.

For Π, Δ, ... etc. electronic states, each rotational level is doubly degenerate (λ-doubling), but one member of the doublet is symmetric and the other is antisymmetric with respect to nuclear exchange, so that for these electronic states, all rotational states occur and are non-degenerate. Thus the factor of $\frac{1}{2}$ is not included in the partition function for $O_2(^1\Delta_g)$, for example.

The value of g_Σ is just

$$g_\Sigma = \frac{h}{B} \frac{d\nu}{dH} \tag{55}$$

The values of $d\nu/dH$ and p have been calculated by Tinkham and Strandberg[33] for many of the O_2 lines.

Westenberg and deHaas[39] have made the corresponding calculation for the composite 6-line O atom spectrum at 300°K, showing that

$$N_O = 0.206 \left(\frac{2kT}{h\nu_o f_+ \beta} \right) I_O \tag{56}$$

(The subscript O indicates O atom.) They have also calculated the numerical values for the proportionality constant Q_O in the equation

$$\frac{N_O}{N_\Sigma} = Q_O \frac{I_O}{I_\Sigma} \tag{57}$$

for several $O_2(^3\Sigma_g^-)$ lines. For line C, $Q_O = 2.02 \times 10^{-3}$.

To determine the $O_2(^1\Delta_g)$ concentration, we return to Eq. (50), using the subscript Δ to identify quantities which apply specifically to $O_2(^1\Delta_g)$.

$$N_\Delta = \frac{kTg_\Delta \beta Z_\Delta}{\nu_o h} \quad \frac{\exp(E_i/kT)}{|\mu_{ij}|^2} \quad I_\Delta \tag{58}$$

From the calculation of the $O_2(^1\Delta_g)$ spectrum, we have $g_\Delta = 2/3$ and $|\mu_{ij}|^2 = 12/9\ b^2 f_+$ for the $M_J = 0 \rightarrow 1$ line. The zero of energy is chosen as the lowest vibrational state of $O_2(^1\Delta_g)$ so that $\exp(E_i/kT) = 1$, and the partition function is

$$Z_\Delta = \frac{kT}{B_\Delta h} \tag{59}$$

Combining Eqs. (53) and (58), we obtain

$$\frac{N_\Delta}{N_\Sigma} = \frac{g_\Delta g_{el}^2 p R_\Sigma}{4\, g_\Sigma B_\Delta} \cdot \frac{I_\Delta}{I_\Sigma}$$

$$= \frac{(0.667)(4)(0.859)(1.45)}{(4)(0.93)(1.43)} \cdot \frac{I_\Delta}{I_\Sigma} \tag{60}$$

$$= 0.624 \quad \frac{I_\Delta}{I_\Sigma}$$

During the actual experiments, only peak height measurements were made because this could be done much more simply and easily than measuring integrated intensities. The experimental $O_2(^1\Delta_g)$ and $O_2(^3\Sigma_g)$ peak heights could not be used as a direct measure of concentration since the widths of these lines were not the same. It was thus necessary to measure experimentally the factor A, defined by

$$\frac{S_\Delta}{S_\Sigma} A = \frac{I_\Delta}{I_\Sigma} \qquad (61)$$

where S_Δ/S_Σ is the ratio of the $O_2(^1\Delta_g)$ peak height to the $O_2(^3\Sigma_g)$ peak height.

For the determination of A, the discharge-flow system was operated in the usual manner, with the discharge excited for $O_2(^1\Delta_g)$ measurements and off for O_2 ground state measurements. The normal phase detector output was recorded and was also connected in parallel to the integrator, so that both the peak height and integrated outputs could be recorded simultaneously. The magnetic field was swept over a large enough range to provide an adequate baseline for the integrated traces. For each set of conditions, the two lines were swept through four times, reversing the sweep direction after each pass. Only the spectrometer gain was changed between the $O_2(^1\Delta_g)$ sweeps and the $O_2(^3\Sigma_g)$ sweeps, and it was always changed by the same amount. The peak heights were measured in the usual way with a ruler, and the integrated traces were integrated a second time with a planimeter. The ratios I_Δ/S_Δ and I_Σ/S_Σ were calculated for each of the four sweeps and these four were averaged. Figure 10 shows the results of the measurement of A as a function of pressure. The error bars represent the typical spread of the four individual measurements. The best straight line through the points has been drawn in.

In a number of experiments, A was measured for mixtures of O_2 with different amounts of He and Ar at constant pressure. These data are shown in Figs. 11 and 12. Within the uncertainties of these measurements, A seemed not to change as the fraction of added rare gas was changed.

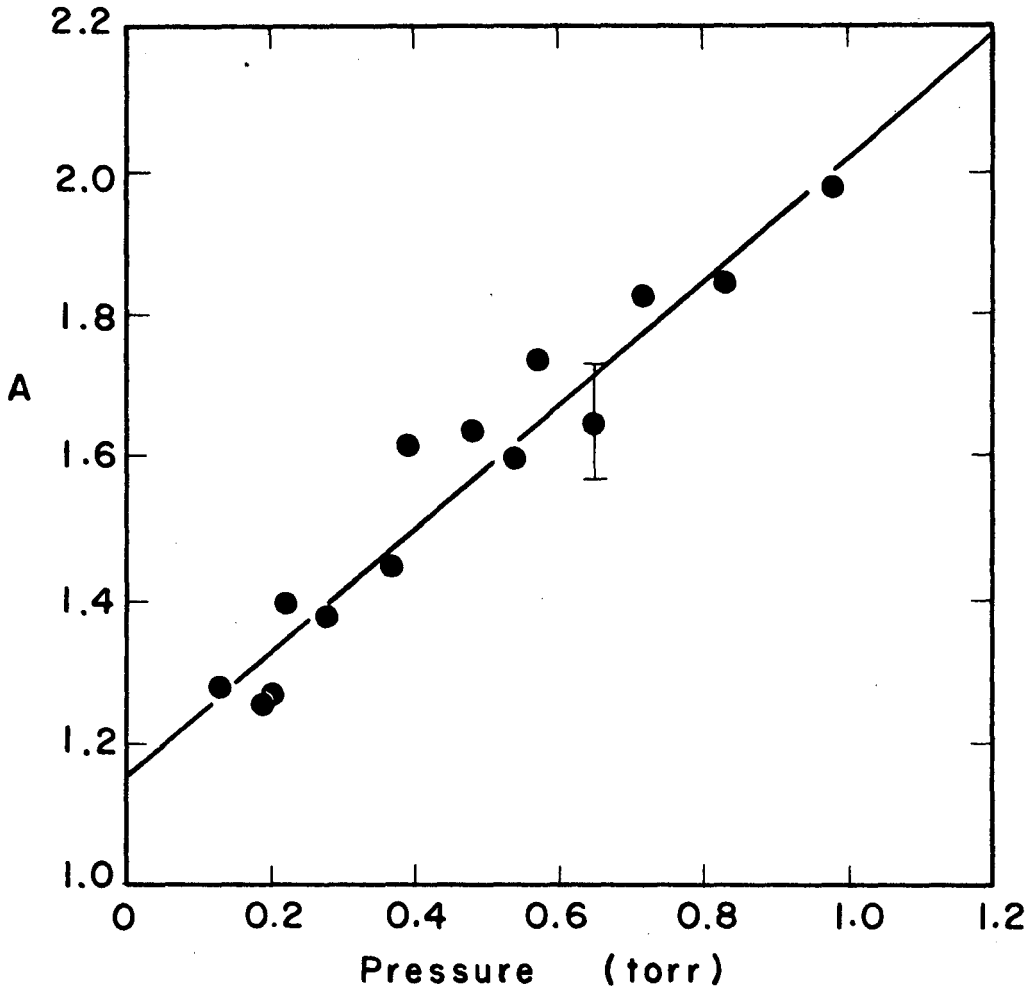

XBL675-3014

Fig. 10 Determination of A as a function of pressure.

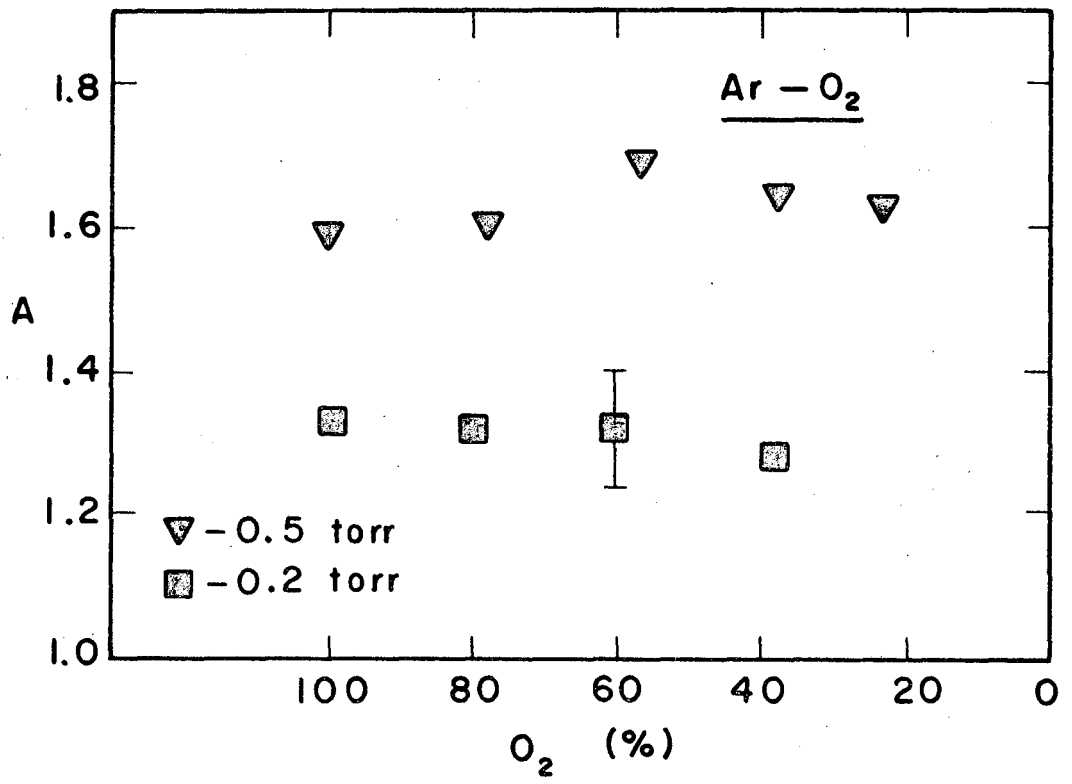

XBL675-3015

Fig. 11 Measurement of A in Ar-O_2 mixtures.

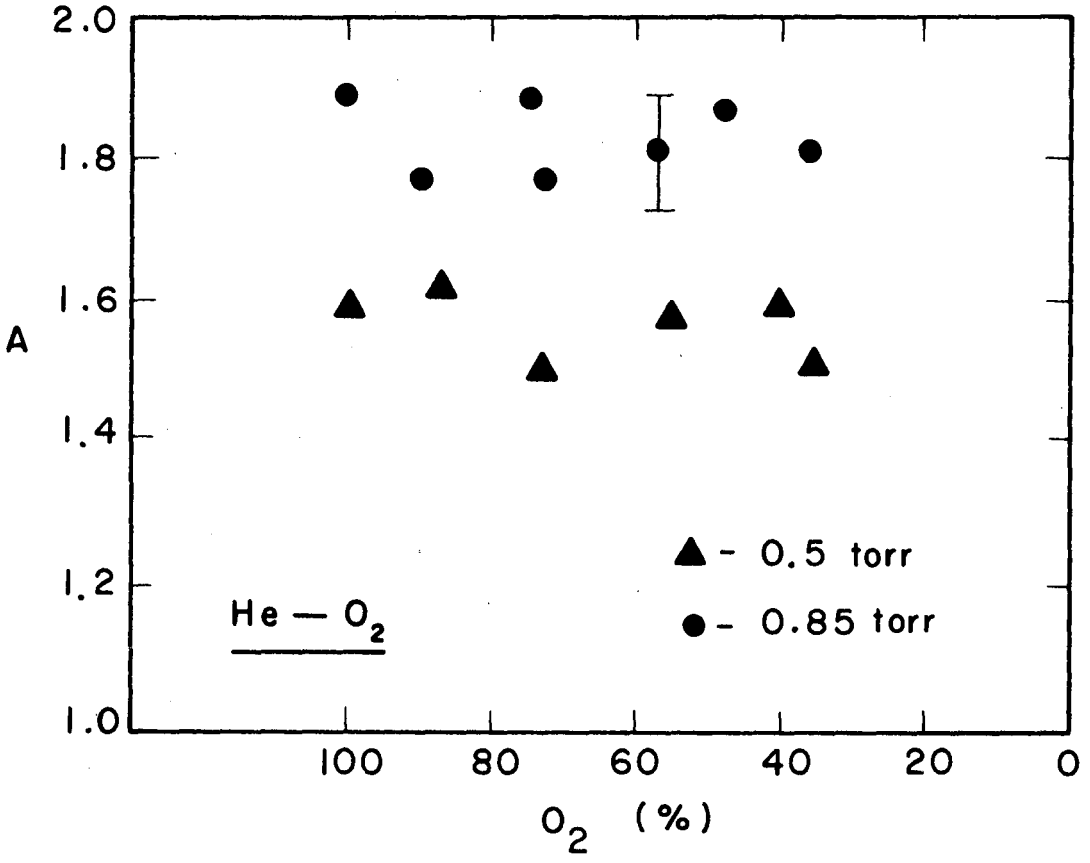

XBL675-3016

Fig. 12 Measurement of A in He-O_2 mixtures.

5. Typical Experimental Procedure

a. Determination of the order of the reaction. A number of runs were made using pure tank O_2 at various pressures to determine the order of the reaction. A constant flow through the system was established and the discharge was started. The EPR spectrometer was set to sweep back and forth across the $M_J = 0 \rightarrow 1$ $O_2(^1\Delta_g)$ line. Each sweep took one minute. Simultaneously, the photomultiplier output was recorded on another recorder which was synchronized with the EPR recorder. After 5 to 10 minutes, the discharge power was changed to a new level for another 5 to 10 minutes. Several more points were taken in this manner for each run. Runs were made using unmixed O_2 at various pressures and also using mixtures of O_2 with different amounts of helium and argon.

b. Relative rate constant measurements. A typical relative rate constant measurement involved the following procedure. With the flow system operating but the discharge turned off, the EPR signal from the $^3\Sigma_g^-$ line A would be swept over several times, each sweep in the opposite direction from the previous one. During this time the pressure was measured with the McLeod gauge, and the signal from the standard light source was measured with the photomultiplier system. Then the discharge was turned on at as low a power as possible while maintaining a steady discharge. Both the $O_2(^1\Delta_g)$ EPR signal and the photomultiplier output were recorded simultaneously for several minutes, the EPR line being swept over once per minute. During this time, and again after every change of discharge power level, the high voltage on the photomultiplier dynodes was removed for several seconds so that the zero level could be measured. This level was not exactly zero because of the Milli-microvoltmeter zero-offset as

well as some pickup from the discharge power source. The discharge power was then increased somewhat and the signals were again measured for the same length of time. In some experiments the higher power was used first. Finally the discharge power was turned off and the standard light signal was remeasured.

B. Results

1. Preliminary Experiments

A few of the earlier experiments performed gave some interesting qualitative results. Small amounts of NO_2 could be added to the discharged oxygen through a second titration inlet (which was later removed) located immediately downstream from the discharge. When sufficient NO_2 was added to completely remove oxygen atoms only a very small diminution of the $O_2(^1\Delta_g)$ EPR signal was noticed, and this could be attributed to dilution effects. Thus $O_2(^1\Delta_g)$ molecules are formed principally in the discharge and not by recombination of atoms downstream. Furthermore, NO and NO_2 react slowly or not at all with $O_2(^1\Delta_g)$. In some experiments double titrations were performed. Oxygen atoms were removed with NO_2 immediately after the discharge, and ethylene was added through the other titration inlet. The $O_2(^1\Delta_g)$ EPR signal was reduced and could be eliminated by the addition of small amounts of ethylene. When ethylene alone was added, the green NO-O afterglow from the discharge could be extinguished without diminishing the $^1\Delta_g$ signal. We conclude that $O_2(^1\Delta_g)$ molecules react with ethylene at a rate which is smaller than that of the ethylene-oxygen atom reaction.

A large number of experiments were performed to determine the order of the reaction

$$2O_2(^1\Delta_g) \rightarrow 2O_2(^3\Sigma_g) + h\nu(6340\text{Å}) \qquad (1)$$

using different pressures between 0.1 and 1.0 torr and various mixtures of oxygen with up to 75% of helium or argon. A second order plot of the results of a typical experiment is shown in Fig. 13. All of the measurements

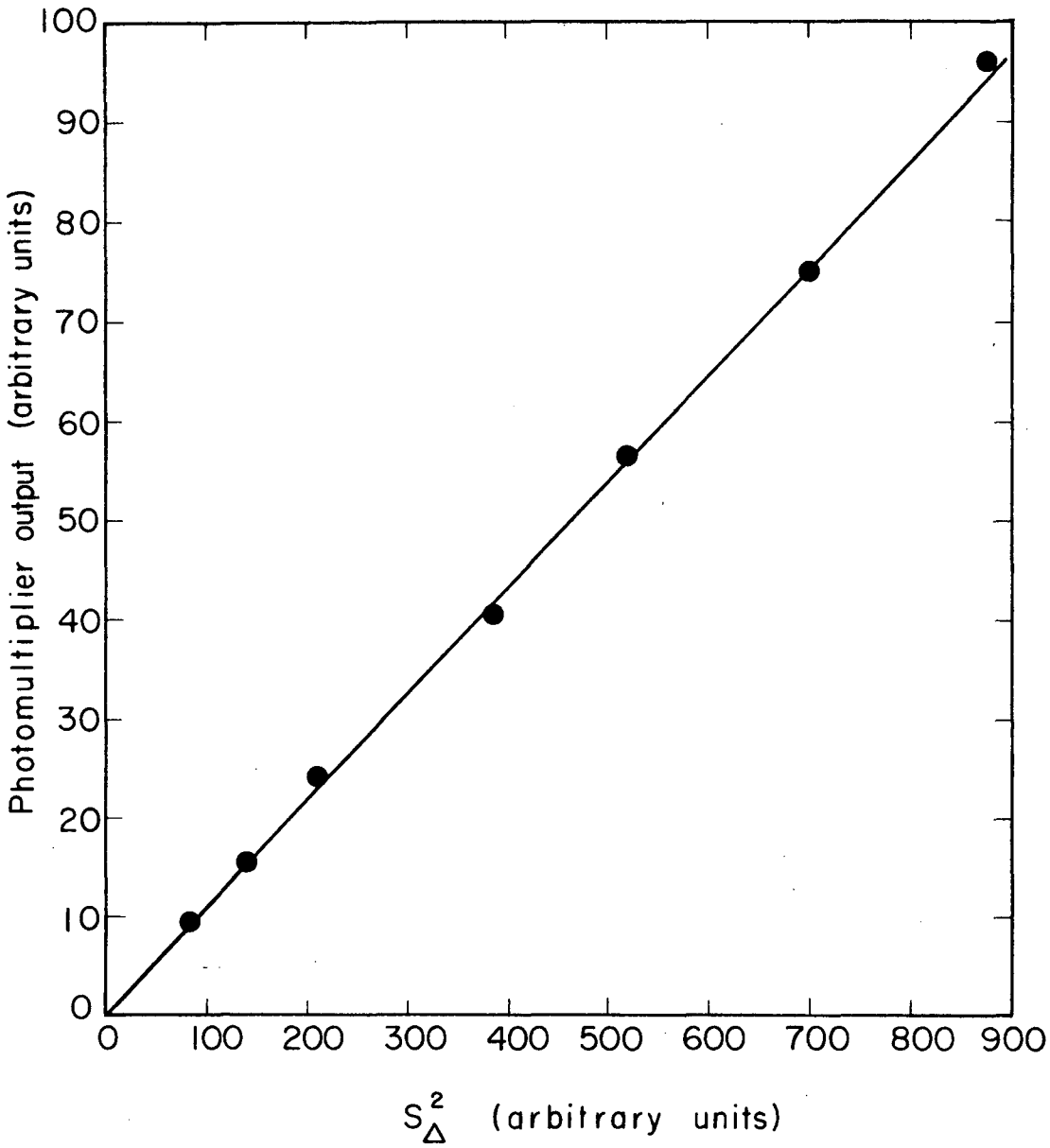

XBL675-3018

Fig. 13 Typical plot of 6340Å emission intensity vs. the square of the $O_2(^1\Delta_g)$ concentration

made showed similar behavior, indicating a second order dependence on the $O_2(^1\Delta_g)$ concentration over a range of at least a factor of three in concentration.

2. Pressure Dependence

The rate constant for reaction 1 was measured as a function of pressure over the range 0.1-1.0 torr. The rate constant was calculated from the expression

$$k = 1.59\times10^{-25} \frac{(\text{slope})(S_\Sigma^2)}{A^2 p^2} \text{ cm}^3/\text{molecule-sec} \qquad (62)$$

The slope in this equation is the change in the experimental photomultiplier voltage divided by the change in the square of the $O_2(^1\Delta_g)$ peak signal height, measured in millimeters. The $O_2(^3\Sigma_g^-)$ calibration peak signal height (in mm) is S_Σ and p is the total pressure in the EPR cavity. The numerical factor contains all of the necessary calibration factors. The value of A used was given by

$$A = 1.16 + 0.856\ p \qquad (63)$$

which is simply the equation of the best straight line through the data of Fig. 10. The results are listed in Table IV and shown in Fig. 14. A number of runs were made using O_2 prepared from $KMnO_4$. The results of these runs were not significantly different from the runs done with tank O_2. Up to about 0.7 torr, the rate constant is independent of pressure within the experimental uncertainty. Above this pressure, the rate appears to decrease somewhat and the scatter of data points increases.

The rate constant was also measured for mixtures of up to 75% He or Ar with oxygen. For these data, p in Eq. (62) is the partial pressure of O_2 in the EPR cavity. The value of A used was that which corresponded

to the total pressure, since A seemed to be unaffected by the addition of He or Ar (see Figs. 11 and 12). The results are presented in Figs. 15 and 16 and in Tables V and VI. The plotted value for 100% O_2 in Fig. 15 is an average value taken from Fig. 14. The 100% value in Fig. 16 is from a run which was done at the same time and under the same flow conditions as the rest of the runs plotted in that figure; the value is somewhat lower than the average from Fig. 14 because of slightly different flow conditions used in this set of runs. This is discussed in detail below.

Table IV. Rate constant measurements in O_2

Run No.	pressure (torr)	$k_1 \times 10^{23}$	O_2 source
112H	0.78	6.95	tank
115B	0.19	7.75	tank
116A	0.19	5.24	$KMnO_4$
116B	0.21	6.84	$KMnO_4$
116C	0.24	7.40	$KMnO_4$
116D	0.29	7.55	$KMnO_4$
116E	0.34	7.07	$KMnO_4$
116F	0.38	7.40	$KMnO_4$
116G	0.45	7.11	$KMnO_4$
117D	0.65	8.04	tank
118B	0.54	9.43	tank
118C	0.74	7.48	tank
118D	0.85	6.26	tank
118E	0.97	5.64	tank
118F	1.23	4.84	tank
119A	0.10	6.67	$KMnO_4$
119B	0.14	7.15	$KMnO_4$
119C	0.16	7.07	$KMnO_4$
119D	0.20	6.95	$KMnO_4$
119F	0.39	8.11	$KMnO_4$
119H	0.62	7.95	$KMnO_4$
119I	0.75	6.35	$KMnO_4$
120A	0.87	7.71	tank
120B	1.01	6.60	tank
123A	0.51	7.67	tank
124A	0.21	7.40	tank
125A	0.86	4.72	tank

Table V. Rate constant measurements in O_2-Ar mixtures

Run No.	pressure (torr)	$k_1 \times 10^{23}$	$\%O_2$	O_2 source
122A	0.50	8.04	68	$KMnO_4$
122B	0.52	7.47	58	$KMnO_4$
122C	0.50	7.51	45	$KMnO_4$
122D	0.50	7.31	30	$KMnO_4$
122E	0.50	7.35	22	$KMnO_4$
123B	0.51	7.47	81	tank
123C	0.51	7.63	61	tank
123D	0.51	7.51	41	tank
124C	0.22	7.11	80	tank
124D	0.22	7.47	59	tank
124E	0.22	7.75	39	tank

Table VI. Rate constant measurements in O_2-He mixtures

Run No.	pressure (torr)	$k_1 \times 10^{23}$	$\%O_2$	O_2 source
125A	0.86	4.72	100	tank
125B	0.77	5.16	70	tank
125C	0.82	4.40	44	tank
125D	0.84	4.60	31	tank
126A	0.80	4.68	48	tank
126B	0.82	4.48	36	tank
126C	0.79	4.36	27	tank

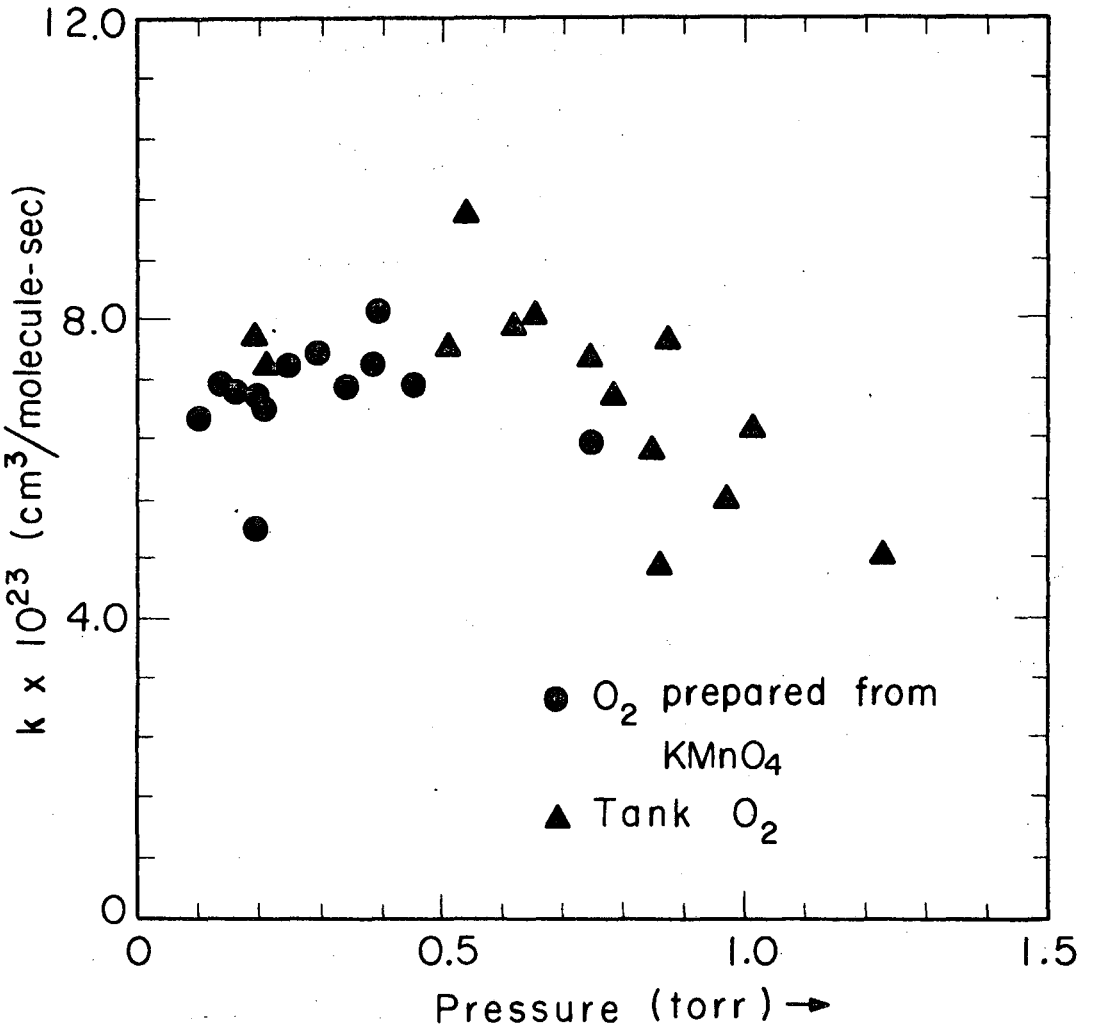

Fig. 14 Measurement of k_1 as a function of pressure

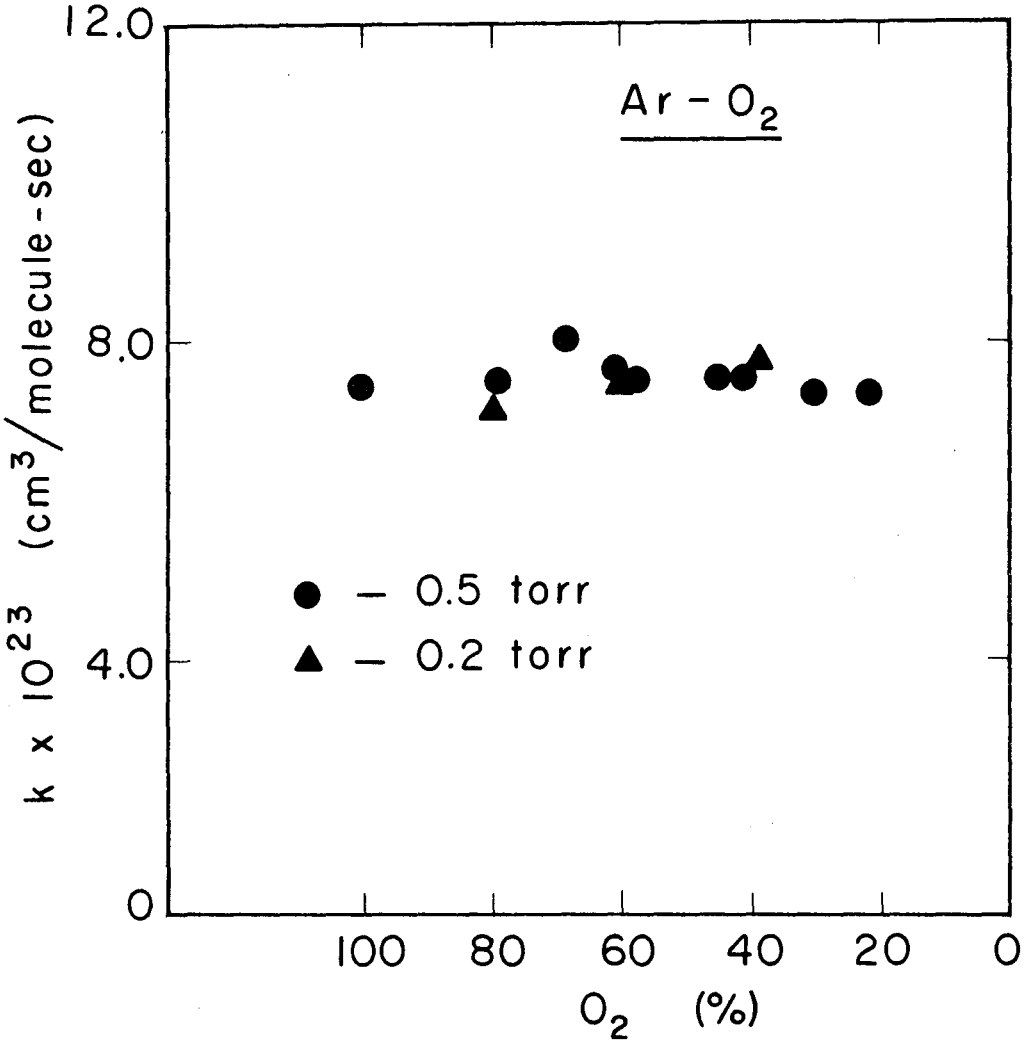

XBL675-3019

Fig. 15 Measurement of k_1 in Ar-O_2 mixtures

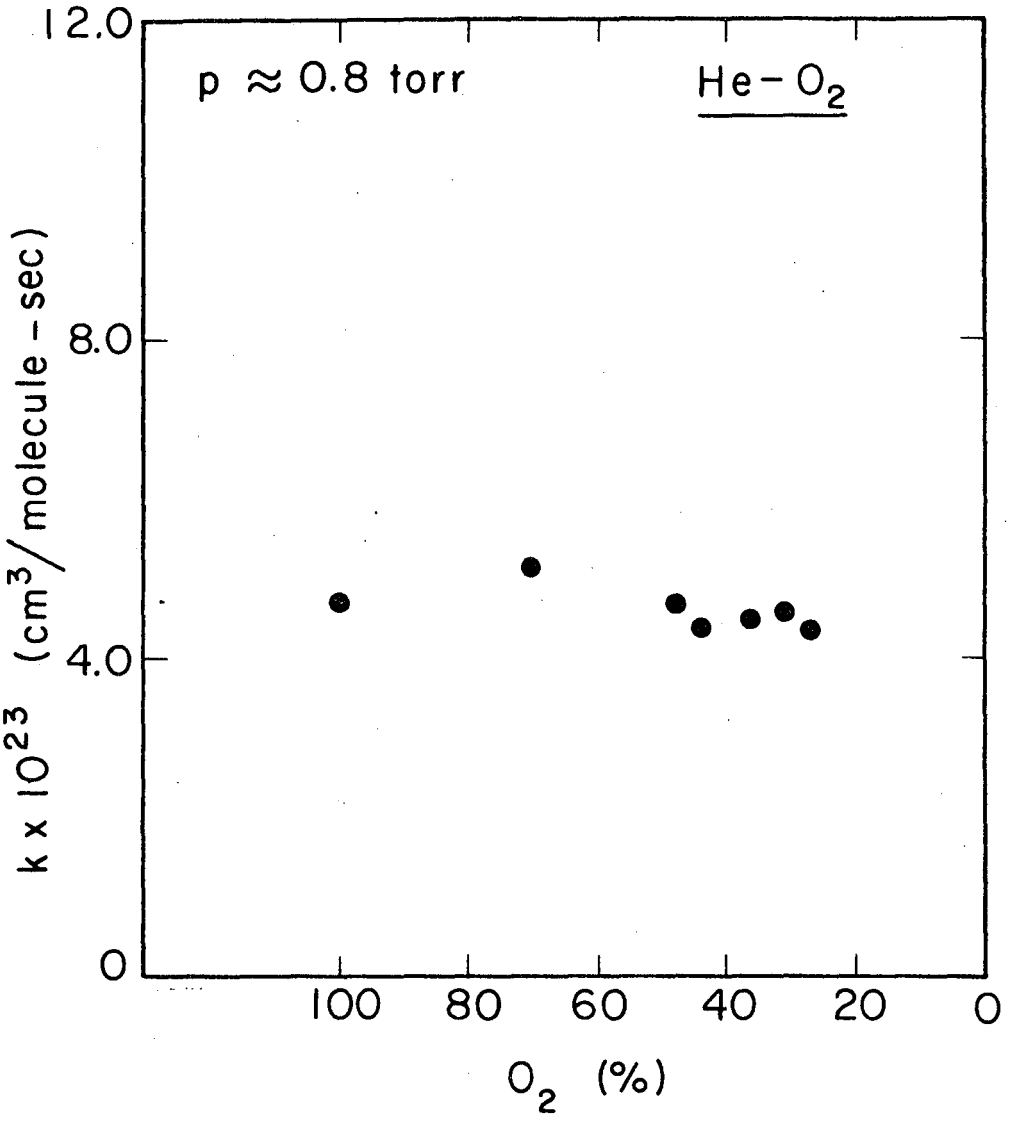

XBL675-3020

Fig. 16 Measurement of k_1 in He-O_2 mixtures

C. Discussion

1. Order of Reaction (1)

Our determination of the order of reaction (1) is in agreement with the results reported by Ogryzlo and co-workers,[13,23] and by Finlay and Whitlow,[24] but differs from the linear relationship found by Schiff, et al.[18] Arnold[13] has suggested that the anomalous result is due to the low and possibly non-linear response of the photomultiplier used by Schiff et al.[18] at 12,680 A to measure the $O_2(^1\Delta_g)$ concentration. We can only add the additional weight of our results to this argument.

2. Pressure Dependence of k_1

It seems very likely that the apparent decrease in k_1 with increasing pressure is not real, particularly in view of the work of Arnold[13] which shows that k_1 is not a function of pressure over the range 1.0-5.2 torr. In addition, it is difficult to imagine a reasonable mechanism whereby the rate constant would fall off as the pressure increased but would be unaffected by the addition of 75% of helium.

Several factors could have caused this effect, probably the most important being small decreases in the system pressure during the course of the higher pressure runs, caused by depletion of the gas in the flow reservoir tank. In Fig. 17, the data for $p > 0.7$ torr are replotted, including the helium mixture data. The plotted points are listed in Table VII. The points are marked as circles were taken in the normal way, that is, the discharge was first set at a low power and the $O_2(^1\Delta_g)$ EPR and light signals were measured; then the power was increased and the signals were remeasured. The double reservoir tank (70 l) was used. The squares were done also with the double tank but in reverse order, the

Table VII. High pressure measurements of k_1

Run No.	pressure (torr)	$k \times 10^{23}$	order	reservoir tank	mixture
112H	0.78	6.95	normal	double	O_2
118D	.85	6.26	normal	double	O_2
118E	.97	5.64	normal	double	O_2
118F	1.23	4.84	normal	double	O_2
120A	.87	7.71	reversed	double	O_2
120B	1.01	6.60	reversed	double	O_2
125A	.86	4.72	normal	single	O_2
125B	.77	5.16	normal	single	O_2+He
125C	.82	4.40	normal	single	O_2+He
125D	.84	4.60	normal	single	O_2+He
126A	.80	4.68	normal	single	O_2+He
126B	.82	4.48	normal	single	O_2+He
126C	.79	4.36	normal	single	O_2+He

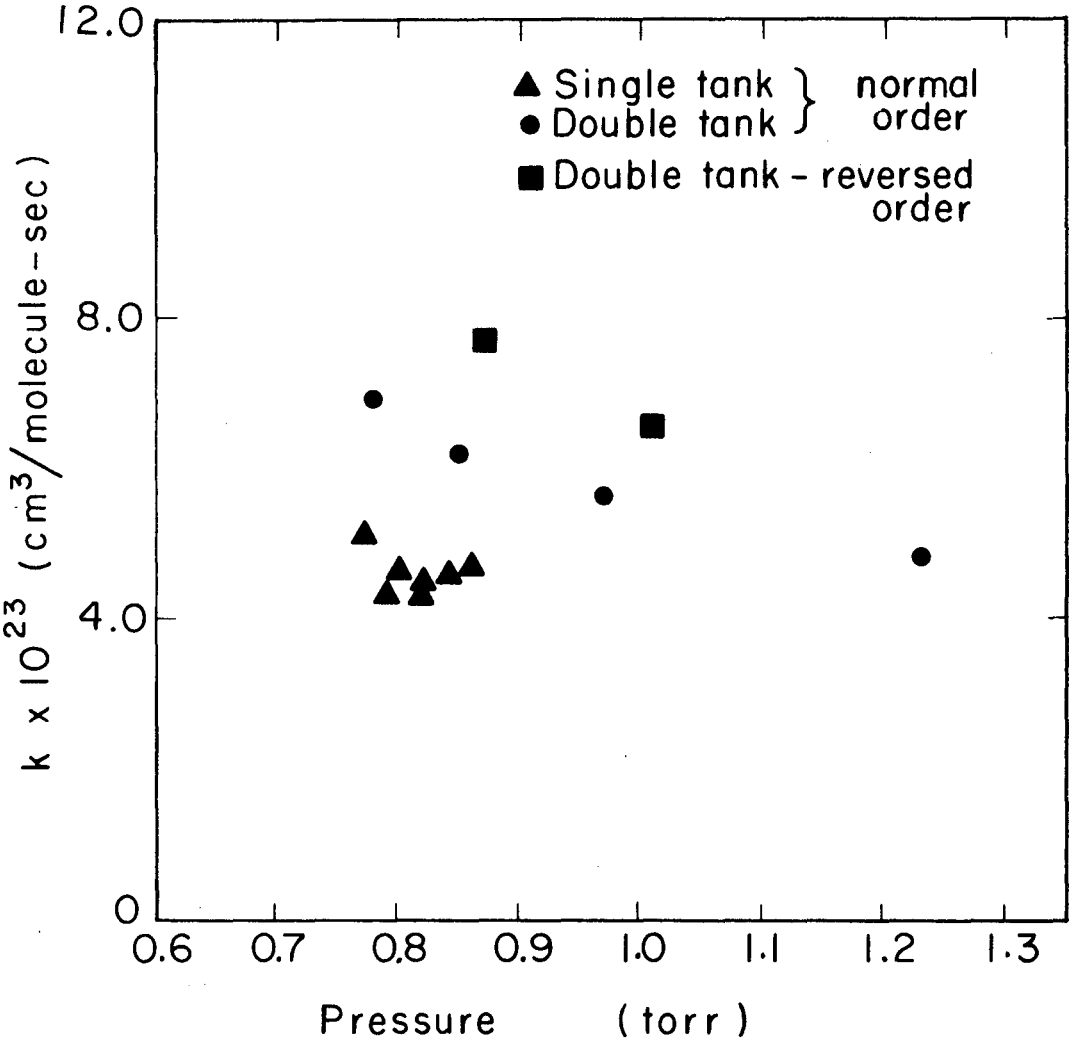

XBL675-3021

Fig. 17 High pressure measurements of k_1

higher power signals being measured first. For the triangles, the measurements were taken in the normal order but only a single 35 l tank was used as a reservoir.

These results can be explained in terms of the following crude model. Let us suppose that the the integrated intensity of an EPR line is proportional to the peak height, S, times the linewidth, W:

$$I = CSW \tag{64}$$

where C is constant. For a Lorentzian line, W is proportional to pressure. If the fractional amount of the species producing the line is independent of pressure, then I will also be proportional to p. Both the results of Arnold[13] and our findings indicate that the fraction of $O_2(^1\Delta_g)$ produced at constant power is relatively constant; therefore one expects S_Δ to be fairly independent of pressure. For the case of pure $O_2(^3\Sigma_g^-)$, S_Σ is in fact nearly constant over quite a large pressure range.[41]

Thus we can write

$$\frac{S_\Delta}{S_\Sigma} A = \frac{I_\Delta}{I_\Sigma} = (\text{const}) \frac{S_\Delta}{S_\Sigma} \frac{p_\Delta}{p_\Sigma} \tag{65}$$

or

$$A = (\text{const}) \frac{p_\Delta}{p_\Sigma} \tag{66}$$

where p_Δ is the average pressure at which the $O_2(^1\Delta_g)$ measurements were made and p_Σ is the pressure at which the $O_2(^3\Sigma_g^-)$ calibration line was measured. The latter measurement was always made before the former ones so that $p_\Delta/p_\Sigma < 1$. At a system pressure of 0.86 torr, using a single reservoir tank, p_Δ and p_Σ differed by about 5%. This would account for about a 10% decrease in the measured value of k_1 at this pressure (because k_1 depends on A^2), or a little less than half of the observed decrease.

A further reduction in k_1 can be attributed to the fact that the pressure also changed slightly between the two $O_2(^1\Delta_g)$ measurements. Our measured rate constant is proportional to $1/(I_2-I_1)^2$ where I_1 is the first (usually lower) $O_2(^1\Delta_g)$ EPR line intensity and I_2 is the second. According to our assumptions, S_2 will be about the same whether the pressure changes or not. Since we assumed the pressure to remain constant in our initial calculation of the rate constant, if it falls slightly between measurements 1 and 2, we have overestimated I_2 and underestimated k_1. The effect is reversed if the higher concentration is measured first. Comparison of the circles and squares plotted in Fig. 17 shows that this effect does indeed seem to be present. Its magnitude seems to be about the same as the effect just discussed, but with only two points any conclusion must be tentative.

Another factor which must be considered is losses of $O_2(^1\Delta_g)$ by reaction or other deactivation processes while traveling from the light cell to the EPR cavity. In our system, one might reasonably expect these losses to occur via processes which are first or second order overall. Some of the possible second order processes are

$$2O_2(^1\Delta_g) \rightarrow O_2(^1\Sigma_g^+) + O_2(^3\Sigma_g^-) \qquad (67)$$

$$O_2(^1\Delta_g) + O_2(^3\Sigma_g^-) \rightarrow 2O_2(^3\Sigma_g^-) \qquad (68)$$

$$2O_2(^1\Delta_g) \rightarrow 2O_2(^3\Sigma_g^-) + h\nu \qquad (69)$$

Arnold[13] has reported a rate constant of 2.2×10^{-18} cm^3/molecule-sec for reaction (67), which is several orders of magnitude larger than the rate constant for process (69) measured in this work and also by Arnold, Browne and Ogryzlo.[23] Consequently, process (69) will account for a

negligible fraction of the losses. Only an upper limit has been reported for reaction (68),[13,16] and we cannot be certain that there are no other second order processes occurring simultaneously which we have neglected. Fortunately, Arnold[13] has measured an upper limit for the rate constant for second order overall losses of $k_{2nd} = 6.0\times10^{-19}$ cm^3/molecule-sec. Using this value we estimate that less than 1/2% of the total $O_2(^1\Delta_g)$ concentration could have been destroyed by these processes while making the journey between the two cells.

Young and Black[19] reported a rate constant of about 3×10^{-14} cm^3/molecule-sec for reaction (67), which appears to be in error. Both Arnold[13] and Winer and Bayes[16] found this value to be several orders of magnitude too large to be consistent with their results. Our data point to a similar conclusion since we observed concentrations in the EPR cavity a factor of 100 larger than would be possible if Young and Black's results were valid. We have therefore assumed that it is incorrect and have omitted it from the discussion above.

First order losses in the system could occur by two processes:

$$O_2(^1\Delta_g) \rightarrow O_2(^3\Sigma_g^-) + h\nu \ (12{,}680A) \qquad (70)$$

$$O_2(^1\Delta_g) \xrightarrow{k_{wall}} O_2(^3\Sigma_g^-) \qquad (71)$$

The measured rate constant for radiative decay (reaction (70)) is 1.5×10^{-4} sec^{-1},[17] so losses due to this reaction will be insignificant. Two measurements of the rate of wall deactivation of $O_2(^1\Delta_g)$ have been reported: Arnold[13] found one deactivation in 10^5 collisions and Winer and Bayes[16] found one in 3.5×10^4 collisions with the wall. The effects of wall deactivation in our system, assuming this to be the primary mode

of decay, are indicated in Table VIII. Concentration ratios, R, defined as

$$R = \frac{O_2(^1\Delta_g) \text{ concentration in light cell}}{O_2(^1\Delta_g) \text{ concentration in EPR cell}} \qquad (72)$$

have been calculated for several pressures and for two values of α, the average number of wall collisions which an $O_2(^1\Delta_g)$ molecule must undergo before being deactivated. The transit time, Δt, is the average time required for a molecule to travel from a point halfway through the light cell to a point halfway through the EPR cell. The effect of a significant amount of wall loss would be to increase the measured rate constant, and from Table VIII it is evident that the effect would be more pronounced at lower pressures. If one again examines Fig. 14, no such trend is observed in the region 0.1-0.6 torr. We can set an upper limit on the possible increase in the rate constant as the pressure is decreased from 0.6 torr to 0.2 torr of about 15%.

This implies that the ratios R do not differ by more than 7-1/2% at the two pressures. Consequently, the minimum average number of wall collisions necessary for deactivation must be about 2×10^5. This is reasonably close to Arnold's value of 10^5 but seems somewhat high compared to Winer and Bayes' result. One might speculate that the use of a reactive olefin in the latter system could have increased the deactivation efficiency of the walls, but there is no real evidence on this point.

If we assume that $\alpha = 2\times10^5$, which corresponds to $k_{wall} = 0.11 \text{ sec}^{-1}$, the measured rate constant would be decreased by only about 4% between 0.6 and 1.0 torr due to wall losses.

The foregoing discussion contains the implicit assumption that k_{wall}

Table VIII. Predicted wall losses of $O_2(^1\Delta_g)$ for different values of α

Total pressure (torr)	flow rate (cm^3/sec)	transit time, Δt (sec)	$R(\alpha = 10^5)$	$R(\alpha = 2\times10^5)$
0.2	230	0.79	1.19	1.09
0.4	430	0.43	1.10	1.05
0.6	560	0.33	1.08	1.04
1.0	850	0.22	1.05	1.02

Total volume = 181 cm^3

Average surface/volume ratio = 2.02

is independent of pressure. This will be true if the average time required for a molecule to diffuse to the wall (t_D) is much smaller than the average time for a molecule to be deactivated at the wall (t_w). The value of t_D can be estimated from the theory of Brownian motion, which gives:[35]

$$t_D = \frac{\overline{x^2}}{2D} \qquad (73)$$

where D is the diffusion coefficient and $\overline{x^2}$ is the mean square particle displacement during the time t_D. The self-diffusion coefficient for O_2 at 273°K and one atmosphere is 0.18 cm^2/sec.[35] At 1.0 torr and 300°K the value would be 140 cm^2/sec. Thus the average time for a molecule to diffuse from the center of a 15mm diameter tube to the wall at 1.0 torr would be 2.0×10^{-3} sec. The average time for deactivation by collision

with a wall is $t_w = 1/k_{wall} = 8.8$ sec. Clearly, the process of wall deactivation is not diffusion limited under these conditions and wall deactivation will indeed be independent of pressure.

At first glance, one might expect that any appreciable amount of wall loss would affect the linearity of the second order plots of which Fig. 13 is an example, thereby giving some clue to its magnitude. However, a closer examination shows that this is not true. Suppose the excited molecule concentration in the light cell is C_1 and the concentration in the EPR cell is C_2. If only first order losses occur between the cells, C_1/C_2 will be constant as long as flow and pressure remain the same. In a second order plot we have essentially a graph of C_1^2 vs C_2^2, therefore the effect of first order losses can only be to change the slope but not to alter the linearity of such plots.

There is still another consideration which has not yet been mentioned, namely, the fact that the pressures in the two measurement cells are not equal because of the flow between them. From Fig. 5 it is seen that Δp is almost exactly equal to 10% of p for pressures up to about 0.4 torr, and then gradually decreases to about 7.7% at p = 1.0 torr. The conductance of the tubing between the McLeod gauge connection and the EPR cavity is 1.74 times as great as the conductance between the light cell and the EPR cavity.[45] Hence the light cell pressure will be from 13.4 to 17.4% higher than the EPR cell pressure. The 4% differential would result in a decrease in the measured rate constant of 8% between 0.4 and 1.0 torr, which when added to the other effects already noted appears to offer a satisfactory explanation for the apparent change in k_1 with pressure in Fig. 14.

The average 15.4% difference in cell pressures means that the average measured rate constant was 33% too high. The average value of k_1 from Fig. 14 is 7.5×10^{-23}. Reduction of this figure by 33% gives the corrected best estimate which is $k_1 = 5.0\pm0.5\times10^{-23}$ cm^3/molecule-sec. Using a calorimetric detector, Arnold, Browne, and Ogryzlo (ABO)[23] found $k_1 = 0.14$ l/mole-sec $= 2.3\times10^{-22}$ cm^3/molecule-sec, roughly a factor of 5 larger than our value.

3. Uncertainties in Results

There is a number of possible sources of error in our measurements. Statistical errors in determining slopes, calibration peak heights, pressure, and the factor A, all contributed to the ±10% error limits quoted above. Typical peak height measurements were reproducible to 2 or 3% so that the slopes were good to about 5%. The photomultiplier readings made a negligible contribution to the slope error. Pressure readings (at pressures below 0.6 torr) and the uncertainty in the slope of the A vs p curve accounted for the remainder of the scatter in the values of k_1.

Probably the largest source of systematic error was in the value of k_{36} used, which was reported to be accurate to within 30%.[34] We note that ABO made use of essentially the same k_{36} in their rate measurement so that this cannot explain any of the difference between their result and ours. There were several possibilities for systematic errors to occur in the measurement of $O_2(^1\Delta_g)$ concentrations, and an error of a factor of two or so would be sufficient to account for the difference between ABO's k_1 and ours. Nevertheless, an error of this magnitude seems unlikely because Arnold,[13] working in the same laboratory and using the same method of detection as ABO, found $O_2(^1\Delta_g)$ concentrations to be

typically 6-8%, almost exactly in agreement with our observations at moderately high discharge power.

Large systematic errors from two other sources may be ruled out as well. The graphically calculated interference filter factors F_1 and F_2 would not be expected to be in error by more than 10 or 20% in view of the straightforward nature of the integrations and the relatively precise data available. The relative sensitivity calibration of the photomultiplier tube involved the product of at most 5 experimental ratios all reproducible to better than 1%, implying a cumulative error of less than 5% from this source.

One is left with the O and NO concentration measurements as possible causes of the discrepancy between the two rate measurements. ABO did not report the total pressure at which their calibration was performed but if we assume the $O_2(^1\Delta_g)$ concentration was 7%, the total pressure would have been 5 torr and the O atom concentration 1.5%, comparable to our measured O atom concentration at the titration port. The pressure in our experiment was, of course, a factor of 10 lower. The fact that the EPR and NO_2 titration measurements were consistent with each other lends additional credence to our atom measurements, but the large amount of wall loss complicates matters somewhat.

4. The O_4^* Complex

All of the available evidence to date strongly suggests that the so-called O_4^* complex is merely a colliding pair of O_2 molecules. The fact that the observed emission bands at 6340 and 7030A are almost exactly half of the wavelengths of the (0-0) and (0-1) transitions of

the $^1\Delta_g \rightarrow {}^3\Sigma_g^-$ system combined with the negative temperature dependence[23] of k_1 indicates an unbound intermediate. The lack of any dependence of k_1 on pressure or added gases implies that the role of any third bodies is minimal.

Bunker[44] has considered the mechanics of a collision of two atoms in detail. A pseudo-equilibrium constant, K_U, for the "reaction"

$$X + X = X_2^* \tag{74}$$

can be calculated by assuming that X_2^* exists when r, the X-X internuclear distance is smaller than some value r_o. It turns out that by far the most important kind of collision in determining K_U is one in which the maximum angular momentum is present which will still allow the "rotational barrier" to be surmounted. In this type of collision, the atoms spend most of their time orbiting around each other at a distance of $r = r_{max}$. By assuming a Maxwell-Boltzmann distribution and using the attractive part of the Lennard-Jones potential, $V = -4\epsilon(\sigma/r)^6$, Bunker has shown that

$$K_U = \frac{9}{2}\sqrt{2\pi}\,\sigma^3\left(\frac{\epsilon}{kT}\right)^{1/2} \tag{75}$$

and

$$r_{max} = \sqrt{2}\,\sigma\left(\frac{\epsilon}{E}\right)^{1/6} \tag{76}$$

and that the interaction energy at r_{max} is E/2, where E is the incident kinetic energy.

Even though these results apply strictly only to atoms, it is interesting to examine the predictions for two colliding O_2 molecules. We need first to obtain reasonable values for the Lennard-Jones parameters ϵ and σ. Several values derived from both viscosity and second virial

coefficient measurements may be found in Hirschfelder, Curtis and Bird;[46] we have simply chosen the average values of $\epsilon/k = 115°K$ and $\sigma = 3.5A$. Using these values and $T = 300°K$, one obtains $K_U = 3.0\times10^{-22}$ cm^3/molecule; and $r_{max} = 4.5A$ for a collision with $E = 3kT/2$.

We must also consider the bound O_2-O_2 pairs. According to Pitzer[59] the number of bound states, n, for a van der Waals pair (assuming a Lennard-Jones potential) is given by

$$n = 0.0350\ \sigma\left(\frac{M\epsilon}{k}\right)^{1/2} \tag{77}$$

where M is the molecular mass in atomic units and k is the Boltzmann constant. For an O_2-O_2 pair, n is about 8, a large enough number to allow the use of the classical phase space integral calculation of Bunker and Davidson[47] who obtained the approximate formula

$$\frac{K_B}{\sigma^3} = \pi^{1/2}\left(\frac{\epsilon}{kT}\right)^{3/2}\left[\frac{8}{3} + \frac{32}{45}\ \frac{\epsilon}{kT}\right] \tag{78}$$

Here, K_B is the equilibrium constant for the formation of bound O_2-O_2 pairs which is found to be $K_B = 5.3\times10^{-23}$ cm^3/molecule with the same Lennard-Jones parameters as above.

We have then the following reaction scheme:

$$\begin{array}{ccccc} O_2^* + O_2^* & \underset{k_b}{\overset{k_a}{\rightleftharpoons}} & O_4^{**} & \underset{k_eM}{\overset{k_dM}{\rightleftharpoons}} & O_4^* \\ & & \downarrow k_c & & \downarrow k_f \\ & & 2O_2 + h\nu & & 2O_2 + h\nu \end{array} \tag{79}$$

where $O_2^* = O_2(^1\Delta_g)$, $O_2 = O_2(^3\Sigma_g^-)$, O_4^{**} is unbound, O_4^* is bound, and M is a third body. Assuming that k_c and k_f are small, one finds that

$$\frac{(O_4^*)}{(O_4^{**})} = \frac{K_B}{K_U} = 0.18 \qquad (80)$$

If both bound and unbound complexes are equally likely to radiate ($k_c = k_f$), and if 6340 and 7030A emissions are equiprobable, then the overall rate constant will be $k_1 = k_c(K_B + K_U)$, so that $k_c = k_f = 0.29$ sec^{-1} and the radiative half life is $0.693/0.29 = 2.4$ sec. This quantity was estimated by ABO to be 0.025 sec on the basis of their experimental value of k_1 and the simple collision theory estimate of

$$K = \frac{k_a}{k_b} = \frac{2\times10^{-10}}{10^{13}} = 2\times10^{-23} \qquad (81)$$

According to Bunker's argument, k_b is probably closer to 10^{12} sec^{-1} which indicates that emission at either 6340 or 7030 A occurs once in 3×10^{12} collisions. In any case, the assumption that k_c and k_f are small is seen to be valid, which means that the concentrations of O_4^* and O_4^{**} are really in equilibrium. This is in agreement with the observed fact that k_1 is independent of pressure or added gases.

Robinson[48] has considered the problem of intensities of forbidden transitions and has shown that a very small interaction energy (about 5 cm^{-1}) between two colliding $O_2(^1\Delta_g)$ molecules would be sufficient to produce all of the observed intensity of the 6340 and 7030 A emissions. The intensity is assumed to be "borrowed" from the relatively intense Schumann-Runge system ($B^3\Sigma_u^- \rightarrow X^3\Sigma_g^-$) by a small amount of collision induced mixing.

Robinson has also pointed out that in liquid O_2 the single $^1\Delta_g \rightarrow {}^3\Sigma_g^-$ transitions occur with about the same intensity as the double transitions. This is reasonable because the intensity of the single transitions is

explained on the basis of exactly the same interaction with the Schumann-Runge system. One would expect this to be true in the gas phase as well, and some evidence on this point has been presented by Badger, Wright and Whitlock[17] who predicted that the reciprocal mean lifetime of $^1\Delta_g$ oxygen molecules subject to decay only by radiative processes first order in $O_2(^1\Delta_g)$ concentration would be

$$\frac{1}{\tau_m} = 2.6\times10^{-4}\ (1 + 3.8P_{O_2})\ \text{sec}^{-1} \qquad (82)$$

where P_{O_2} is the partial pressure of O_2 in atmospheres. Using the second term of this expression, one finds that for the process

$$O_2(^1\Delta_g) + O_2(^3\Sigma_g^-) \rightarrow 2O_2(^3\Sigma_g^-) + h\nu\ (12{,}680\text{A}) \qquad (83)$$

the rate constant would be 4×10^{-23} cm^3/molecule-sec.

The interaction energy between two O_2 molecules at a distance of $r_{max} = 4.5$ A is about $3kT/4 = 160$ cm^{-1} for an average collision.[44] For a bound complex the energy is somewhat larger, obviously a great deal more than Robinson's 5 cm^{-1} in both cases. Since the $O_2(^1\Delta_g \rightarrow {}^3\Sigma_g^-)$ transition occurs by magnetic dipole radiation[11] is would seem that the magnetic dipole-dipole interaction between the two O_2 molecules might be important. For two classical ideal magnetic dipoles, the interaction energy is given approximately by[46]

$$V = \frac{\mu_a\mu_b}{r_{ab}^3}\left[-2\cos\theta_a\cos\theta_b + \sin\theta_a\sin\theta_b\cos(\phi_b-\phi_a)\right] + O\left(\frac{1}{r_{ab}^5}\right) \qquad (84)$$

where μ_a and μ_b are the two magnetic dipole moments whose centers are separated by a distance r_{ab}. The angles θ and ϕ are defined in

Hirschfelder, Curtis and Bird.[46] The maximum energy of interaction between two $O_2(^1\Delta_g)$ molecules via their magnetic dipoles is then:

$$V_{max} = \frac{4\beta^2}{r_{ab}^3} \cdot 2 = \frac{3.5}{r_{ab}^3} \text{ cm}^{-1} \qquad (85)$$

when r_{ab} is given in angstroms. The maximum interaction energy at a distance of 4A, the approximate bound complex distance, is seen to be only about 0.05 cm^{-1}. Even for very strong collisions where r_{ab} = 2.5 A and the repulsive potential is about 18,000 cm^{-1}, V_{max} is only 0.22 cm^{-1}. We must conclude that this interaction is probably not very significant in inducing emission.

5. EPR Concentration Measurements with Inhomogeneously Broadened Lines

Several authors have discussed the measurement of relative and absolute concentrations in the gas phase with EPR.[37,39,42,50-56] The usual assumption which is made in this case is that we are dealing with unsaturated Lorentzian ("pressure broadened") lines. Normally, this assumption is quite valid, but unfortunately it is not for the experiments described here. Due to the large sample volume and high magnetic fields used, the variation in the dc magnetic field over the sample volume was large enough to make inhomogeneous broadening an important factor in the experimental lineshapes. In view of this situation, it is necessary to carefully examine the basis of our concentration measurements.

We wish to show first that the ratio of the doubly integrated spectrometer signals for two species is proportional to the ratio of their true integrated intensities. True integrated intensity is defined as:

$$I = \int_0^\infty \chi''(H)\, dH \qquad (86)$$

We have already seen (Eq. 50) that the true integrated intensity is independent of the lineshape function for an unsaturated, unmodulated line. Our observed lines were, in fact, unsaturated, but it is necessary to consider the effect of modulation on the lineshape and intensity. The modulation and phase detection system used in a typical EPR spectrometer result in an experimental signal which is related to the derivative of $\chi''(H)$. For infinitely small modulation amplitudes the output signal is exactly proportional to $d\chi''/dH$ but as the modulation amplitude is increased, the shape becomes distorted and broadened.[57] In order to realize the maximum sensitivity of the spectrometer, it is necessary to use modulation amplitudes of the order of the linewidth, at which point there is appreciable distortion. Barth, Hildebrandt and Patapoff[54] and Wahlquist[55] have determined analytically the relationships between the relevant quantities for Lorentzian lines at all modulation amplitudes. They showed that the experimental integrated intensity I_{exp} (the doubly integrated spectrometer signal) is equal to the modulation amplitude H_ω times the true integrated intensity I for any value of H_ω. This relationship will be valid for inhomogeneity broadened lines as well, under certain conditions.

Under the experimental conditions used in these experiments, the main intrinsic source of broadening is molecular collisions.[41] Thus if it were possible to view the signal from only a small volume element within the cavity, we would expect to see a modulation broadened Lorentzian line, provided that we had chosen a volume small enough to have a homogeneous magnetic field. If we divide the entire sample volume into i such small elements, the experimentally observed line can be thought of

as the sum of a large number of modulation broadened Lorentzian lines which are nearly, but not exactly, coincident. For each of these lines, we can say that

$$(I_{exp})_i = H_\omega I_i \tag{87}$$

and that

$$I_i = \int_0^\infty \chi_i'' (H)dH = \frac{a_i n_i \omega_0 \hbar}{VkTg_{eff}\mu_0 Z} \; e^{-E_i/kT} \; |\mu_{ij}|^2 \tag{88}$$

$$\equiv a_i n_i C \tag{89}$$

where the subscript i means that the quantity refers only to the ith volume element, which contains n_i absorbing molecules. The total volume of the cavity is V. The filling factors a_i must be included to account for the fact that the signal due to a number of molecules within a small volume would not be the same as the signal from the same number of molecules evenly dispersed in the entire cavity, even assuming a completely uniform dc magnetic field. This will be so because the microwave magnetic field, H_1, will not be the same at all points in the cavity. For gas phase samples, which load the cavity very little and always fill it in the same way, the filling factors will be essentially constant. It is true that H_1 changes slightly when a resonance is excited in the cavity but this change is normally very small[58] (which is one reason that modulation and phase detection are used). The filling factors depend on the total value of H_1, whereas the signal detected depends only on the small changes in H_1.

The total observed integrated intensity will be

$$I_{exp} = \sum_i (I_{exp})_i = H_\omega C \sum_i a_i b_i n_i \qquad (90)$$

The modulation amplitude, like the microwave magnetic field, will not be uniform over the sample. The factors b_i take this into account in an exactly analogous way. For the usual gas phase samples, they will be independent of any property of the sample.

Let us now consider the ratio of the measured intensity of a line due to species X to one due to species Y at constant modulation amplitude:

$$\frac{(I_{exp})_X}{(I_{exp})_Y} = \frac{C_X}{C_Y} \cdot \frac{\sum_i a_i b_i x_i}{\sum_i a_i b_i y_i} \qquad (91)$$

where x_i and y_i represent the numbers of molecules of X and Y in the ith volume element. Since the distribution of the gaseous sample in the cavity will be homogeneous, it will be true in each volume element that

$$\frac{x_i}{y_i} = R \qquad (92)$$

where R is the ratio of the total concentration of X to the total concentration of Y. Substituting for x_i,

$$\frac{(I_{exp})_X}{(I_{exp})_Y} = \frac{C_X}{C_Y} \cdot \frac{R \sum a_i b_i y_i}{\sum a_i b_i y_i} = R \frac{C_X}{C_Y} \qquad (93)$$

From Eq. (50), the ratio of true integrated intensities can be written

$$\frac{I_X}{I_Y} = \frac{C_X N_X}{C_Y N_Y} = \frac{C_X}{C_Y} R \qquad (94)$$

Therefore, within the limits defined by our assumptions, the two intensity

ratios are the same.

a. Peak signal height measurements. The most conveniently measured quantity for comparing concentrations of the same species is the peak signal height, S_p, which is the maximum height of the spectrometer signal at one of the peaks of the derivative curve. Barth, Hildebrandt and Pata-poff[54] and Wahlquist[55] have shown that for a modulation broadened Lorentzian line, the spectrometer signal S(H) will be equal to

$$S(H) = C_2 H_{1/2} N \cdot U(H_\omega, H_{1/2}, H) \qquad (95)$$

where $H_{1/2}$ is the half width at half height of the true absorption line. This half width is determined by the average number of collisions which the absorbing molecule undergoes per second, and the effectiveness of each collision as a relaxation process. This means that the half width may change as the composition of the sample changes. We return to this point shortly. The function U is essentially a shape function, but it is not normalized. The constant C_2 depends on fundamental and instrumental constants and the matrix element for the particular transition. For a Lorentzian line then, it is clear that if the half width remains constant, S(H) will be proportional to $\bar{N}$ at any value of H near resonance. Of course, if H is too far from resonance S(H) will simply be zero.

If we again consider a composite inhomogeneously broadened line, the peak signal height will be the sum of the signals from each of its components:

$$S_p(\text{at } H = H_p) = \sum_i a_i b_i S_i (H_p - H_i) \qquad (96)$$

where H_p is the field at which the experimental peak signal height occurs,

and H_i represents the small offset which each of the components may have due to the dc magnetic field inhomogeneity. If each of the i component lines corresponds to N_i molecules, then

$$S_p = C_2 H_{1/2} \sum_i a_i b_i n_i U_i (H_p - H_i) \tag{97}$$

By an argument identical with that used for the integrated intensities, it is seen that S_p will be proportional to the concentration of the absorbing species. This conclusion is supported by some experimental results obtained by Barth, Hildebrandt and Patapoff,[54] which suggest that inhomogeneously broadened and composite lines obey the equations for single Lorentzian lines if they are sufficiently modulation broadened.

One of the necessary conditions mentioned above for S_p to be proportional to concentration is that $H_{1/2}$ and hence, strictly, the composition of the bulk sample must remain constant. This is a rather severe requirement, since if the concentration of absorbing molecules changes, so does the bulk composition. Krongelb and Strandberg[42] have discussed this problem for a mixture of oxygen atoms in O_2. For the usual Lorentzian line, the shape function is given by

$$F(\omega-\omega_0) = \pi^{-1} \frac{\tau}{1+\tau^2(\omega-\omega_0)^2} \tag{98}$$

The quantity τ is the average time between collisions of an absorbing molecule, which can be written

$$\frac{1}{\tau} = \sigma \bar{v} N = (\text{const}) H_{1/2} \tag{99}$$

Here σ is the collision cross section of the molecule and $\bar{v}$ is the average relative velocity of two colliding molecules. For a mixture of

two gases, A and B, the collision frequency for A molecules will be

$$\frac{1}{\tau_A} = \sigma_{AB}\,\bar{v}_{AB}\,N_B + \sigma_{AA}\,\bar{v}_{AA}\,N_A \qquad (100)$$

where σ_{AA} and σ_{AB} are the cross sections for A-A and A-B collisions, respectively; $\bar{v}_{AA}$ and $\bar{v}_{AB}$ are the corresponding relative velocities; and N_A and N_B are the concentrations of A and B. Substitution gives

$$\frac{1}{\tau_A} = \left[\sigma_{AA}\,\bar{v}_{AA} - \sigma_{AB}\,\bar{v}_{AB}\right]\alpha N + \left[\sigma_{AB}\,\bar{v}_{AB}\right] N \qquad (101)$$

where α is the fraction of molecules which are of type A. The second term is constant. For our experiments, type A molecules are $O_2(^1\Delta_g)$. The fraction of molecules in this state was always less than about 10%, so that the first term will always be small. Also, for the case of $O_2(^1\Delta_g)$ in $O_2(^3\Sigma_g^-)$ one would expect that the differences in collision cross sections would be quite small. For experiments in which He and Ar were used, the situation is slightly more complicated, but here again only the relative concentrations of $O_2(^1\Delta_g)$ and $O_2(^3\Sigma_g^-)$ are changing so that the changes in $H_{1/2}$ should be small in these cases as well. Krongelb and Strandberg[42] found that for 10% or less O atoms in O_2, τ was constant within the accuracy of their measurements.

ACKNOWLEDGEMENTS

I am greatly indebted to Professor Bruce H. Mahan whose helpful advice and encouragement made this research both possible and profitable.

I am grateful to Professor Rollie J. Myers for a number of valuable discussions and a considerable amount of assistance with some of the calculations.

Many of my colleagues are due thanks for their aid and comfort on numerous occasions.

Fellowship aid from the National Science Foundation is gratefully acknowledged.

This work was supported by the United States Atomic Energy Commission through the Lawrence Radiation Laboratory.

REFERENCES

1. F. Kaufman, in Progress in Reaction Kinetics, Vol. I (Pergamon Press, New York, 1961).
2. S. N. Foner and R. L. Hudson, J. Chem. Phys. 25, 601 (1956).
3. J. T. Herron and H. I. Schiff, Can. J. Chem. 36, 1159 (1958).
4. L. Elias, E. A. Ogryzlo, and H. I. Schiff, Can. J. Chem. 37, 1680 (1959).
5. F. Kaufman and J. R. Kelso, Disc. Faraday Soc. 37, 26 (1964).
6. A. Mathias and H. I. Schiff, Disc. Faraday Soc. 37, 38 (1964).
7. L. W. Bader and E. A. Ogryzlo, Disc. Faraday Soc. 37, 46 (1964).
8. M. A. A. Clyne, B. A. Thrush and R. P. Wayne, Nature 199, 1057 (1963).
9. M. A. A. Clyne, B. A. Thrush and R. P. Wayne, Photochem. and Photobiol. 4, 957 (1965).
10. G. Herzberg, Spectra of Diatomic Molecules (D. Van Nostrand Co., New York, 1950).
11. L. Herzberg and G. Herzberg, Astrophys. J. 105, 353 (1947).
12. J. H. Van Vleck, Astrophys. J. 80, 161 (1934).
13. J. S. Arnold, Ph. D. Thesis, University of British Columbia, 1966.
14. C. S. Foote and S. Wexler, J. Am. Chem. Soc. 86, 3879 (1964).
15. E. J. Corey and W. J. Taylor, J. Am. Chem. Soc. 86, 3881 (1964).
16. A. M. Winer and K. D. Bayes, J. Phys. Chem. 70, 302 (1966).
17. R. M. Badger, A. C. Wright, and R. F. Whitlock, J. Chem. Phys. 43, 4345 (1965).
18. R. E. March, S. G. Furnival and H. I. Schiff, Photochem. and Photobiol. 4, 971 (1965).

19. R. A. Young and G. Black, J. Chem. Phys. 42, 3740 (1965).

20. H. U. Kurzweg, A. Bass, and H. P. Broida, J. Mol. Spectr. 1, 184 (1957).

21. H. H. Seliger, Analyt. Biochem. 1, 60 (1960).

22. A. U. Khan and M. Kasha, J. Chem. Phys. 39, 2105 (1963).

23. J. S. Arnold, R. J. Browne, and E. A. Ogryzlo, Photochem. and Photobiol. 4, 963 (1965).

24. F. Finlay and S. Whitlow, Tech. Rept. Defense Research Board of Canada, CARDE T. R. 545/66.

25. J. W. Ellis and H. O. Kneser, Z. Physik. 86, 583 (1933).

26. H. Salow and W. Steiner, Z. Physik 99, 137 (1936).

27. V. I. Dianov-Klokov, Opt. i. Spectr. 6, 290 (1959).

28. E. A. Ogryzlo, J. Chem. Ed. 42, 647 (1965).

29. L. Pauling and E. B. Wilson, Jr., Introduction to Quantum Mechanics (McGraw-Hill Book Co., New York, 1935).

30. M. W. P. Strandberg, Microwave Spectroscopy (Methuen and Co., London, 1954).

31. K. O. Bowers, R. A. Kamper and C. O. Lustig, Proc. Roy. Soc. (London) 251A, 565 (1959).

32. H. E. Radford and V. W. Hughes, Phys. Rev. 114, 1274 (1959).

33. M. Tinkham and M. W. P. Strandberg, Phys. Rev. 97, 951 (1955).

34. A. Fontijn, C. B. Meyer and H. I. Schiff, J. Chem. Phys. 40, 64 (1964).

35. R. D. Present, Kinetic Theory of Gases (McGraw-Hill Book Co., New York, 1958).

36. B. P. Levitt, J. Chem. Phys. 42, 1038 (1965).

37. N. Edelstein, A Study of the Kinetics of the Reaction H + O_2 by Paramagnetic Resonance, Lawrence Radiation Laboratory Report, UCRL-10108, April 1962.

38. D. H. Levy, The Electron Spin Resonance Spectra of Radical Anions in Liquid Ammonia, Lawrence Radiation Laboratory Report, UCRL-11864, January 1965.

39. A. A. Westenberg and N. deHaas, J. Chem. Phys. 40, 3087 (1964).

40. C. P. Slichter, Principles of Magnetic Resonance (Harper and Row, New York, 1963).

41. C. H. Townes and A. L. Schawlow, Microwave Spectroscopy (McGraw-Hill Book Co., New York, 1955).

42. S. Krongelb and M. W. P. Strandberg, J. Chem. Phys. 31, 1196 (1959).

43. T. L. Hill, Introduction to Statistical Thermodynamics (Addison-Wesley, Reading, Massachusetts, 1960).

44. D. L. Bunker, J. Chem. Phys. 32, 1001 (1960).

45. A. H. Turnbull, R. S. Barton and J. C. Riviere, An Introduction to Vacuum Technique (J. Wiley and Sons, New York, 1962).

46. J. O. Hirschfelder, C. F. Curtis and R. B. Bird, Molecular Theory of Gases and Liquids (J. Wiley and Sons, New York, 1954).

47. D. L. Bunker and N. Davidson, J. Am. Chem. Soc. 80, 5090 (1958).

48. G. W. Robinson, J. Chem. Phys. 46, 572 (1967).

49. M. A. A. Clyne and B. A. Thrush, Proc. Roy. Soc. (London) A269, 404 (1962).

50. A. A. Westenberg and N. deHaas, J. Chem. Phys. 46, 490 (1967).

51. A. F. Hildebrandt, F. B. Booth and C. A. Barth, Planetary and Space Sci. 3, 194 (1961).

52. A. F. Hildebrandt, F. B. Booth and C. A. Barth, J. Chem. Phys. 31, 273 (1959).

53. T. C. Marshall, Phys. Fluids 5, 743 (1962).

54. C. A. Barth, A. F. Hildebrandt and M. Patapoff, Disc. Faraday Soc. 33, 162 (1962).

55. H. Wahlquist, J. Chem. Phys. 35, 1708 (1961).

56. B. J. Wood, J. S. Mills and H. Wise, J. Phys. Chem. 67, 1462 (1963).

57. D. J. E. Ingram, Free Radicals as Studied by Electron Spin Resonance (Butterworths Scientific Publications, London, 1958).

58. G. Feher, Bell. Syst. Tech. J. 36, 449 (1957).

59. K. S. Pitzer, Quantum Chemistry (Prentice-Hall, Englewood Cliffs, New Jersey, 1953).